Journal of Computational Physics 229 (2010) 3864–3883

Contents lists available at ScienceDirect

Journal of Computational Physics

journal homepage: www.elsevier.com/locate/jcp

A hybrid numerical method for interfacial fluid flow with soluble surfactant

M.R. Booty *, M. Siegel

Department of Mathematical Sciences, Center for Applied Mathematics and Statistics, New Jersey Institute of Technology, Newark, NJ 07102, USA

ARTICLE INFO

Article history:
Received 19 August 2009
Received in revised form 21 December 2009
Accepted 24 January 2010
Available online 2 February 2010

Keywords:
Hybrid numerical method
Interfacial fluid flow
Soluble surfactant

ABSTRACT

We address a significant difficulty in the numerical computation of fluid interfaces with soluble surfactant that occurs in the physically representative limit of large bulk Peclet number *Pe*. At the high values of *Pe* in typical fluid-surfactant systems, there is a transition layer near the interface in which the surfactant concentration varies rapidly, and large gradients at the interface must be resolved accurately to evaluate the exchange of surfactant between the interface and bulk flow. We use the slenderness of the layer to develop a fast and accurate 'hybrid' numerical method that incorporates a separate, singular perturbation analysis of the dynamics in the transition layer into a full numerical solution of the interfacial free boundary problem. The accuracy and efficiency of the method is assessed by comparison with a more 'traditional' numerical approach that uses finite differences on a curvilinear coordinate system exterior to the bubble, without the separate transition layer reduction. The traditional method implemented here features a novel fast calculation of fluid velocity off the interface.

1. Introduction

Surfactants, or surface contaminants, significantly alter the interfacial properties of a fluid by changing surface tension. A striking example is the tipstreaming of thin threads or small droplets from a drop or bubble that is stretched in an imposed extensional flow. Although first observed by Taylor [1] in his seminal four-roller mill experiments, tipstreaming has only recently been ascribed to the presence of surfactant [2–4], and surfactant mediated tipstreaming has now been utilized to synthesize micron-sized and smaller droplets in a flow focusing device [5]. Other applications of surfactants include their addition to two-phase mixtures or emulsions to facilitate breakup of large droplets and prevent coalescence of smaller ones, thereby stabilizing the emulsion [6]. In medicine, surfactant treatments may reduce risks from gas bubbles in the blood (embolisms) formed during cardiac surgery or rapid decompression, and are used in the reopening of collapsed pulmonary airways [7,8].

Most previous computational studies of the effect of surfactant in interfacial flow are for surfactant that is insoluble, that is, confined to the interface alone. The evolution of surfactant concentration is then determined by a combination of surface fluid velocity, surface diffusion and local stretching or contraction of the interface. Under the simplification of low Reynolds number flow, the evolution is entirely described by surface quantities, and can be solved by surface-based methods such as the boundary integral method [9]. This is among the most accurate and efficient numerical methods for solving free and moving boundary problems.

Boundary integral simulations of the effect of insoluble surfactant on the deformation and breakup of axisymmetric drops in extensional flow by Stone and Leal [10] characterize the dependence of drop deformation on the capillary number $Q = \mu G a/\sigma_0$, where G is the imposed strain rate, σ_0 is the surface tension of a clean or surfactant-free interface, a is the

* Corresponding author.
E-mail addresses: booty@njit.edu (M.R. Booty), misieg@njit.edu (M. Siegel).

0021-9991/$ - see front matter © 2010 Elsevier Inc. All rights reserved.
doi:10.1016/j.jcp.2010.01.032

undeformed radius of the drop, and μ is the suspending liquid viscosity. They consider the case when the ratio $\lambda = \mu_i/\mu$ of drop to suspending liquid viscosity is one, but the simulations were later generalized by Milliken et al. [11] to include different viscosity ratios. The most interesting behavior was observed for nearly inviscid drops $\lambda \ll 1$, when surfactant was found to advect with the stretching flow to the drop ends, which become pointed due to the lower surface tension there. Above a critical capillary number the drop appears to stretch very quickly, but tipstreaming was not resolved due to the near singularity in curvature at the drop ends. Volume-of-fluid (VOF) simulations [12] for low viscosity ratio drops with insoluble surfactant show similar behavior. Droplets or small drop fragments appear to be emitted from pointed bubble tips but are on the scale of the mesh spacing and are therefore not properly resolved, so that tipstreaming may have been introduced as a numerical artifact. Related VOF studies are [13,14]. To our knowledge, the only resolved numerical calculations showing drop shapes with pointed tips from which thin threads are emitted, evoking the tipstreaming observed in experiments, are the boundary integral simulations of Eggleton et al. [3] and Bazhlekov et al. [15]. Tipstreaming behavior has also been observed in boundary integral simulations of two dimensional flow [16–18].

The above results underscore the need to accurately resolve regions of high interfacial curvature in calculations of bubble and drop dynamics, for which boundary integral methods are ideally suited. Other boundary integral studies of drop evolution with insoluble surfactant include [19–23]. Immersed boundary methods [24–26] and the level set method [27] have also been applied to study the effect of insoluble surfactant on the dynamics of fluid interfaces.

The computational challenges of simulating interfacial flow with surfactant are compounded when the surfactant is soluble. A soluble surfactant advects and diffuses as a passive scalar in the bulk fluid, but there is an exchange or transfer of surfactant between its dissolved form in the bulk and its adsorbed form on the interface. Gradients of bulk surfactant concentration near the interface must be accurately computed to properly account for the exchange of surfactant between its dissolved and adsorbed forms.

In this paper, we address a significant difficulty in the numerical computation of fluid interfaces with soluble surfactant that occurs in the practically important limit of large bulk Peclet number *Pe*. The Peclet number *Pe* measures the ratio of bulk advective to diffusive transport, and its value in typical systems varies from 10^5 to 10^6 [28,29]. At these high values of *Pe*, there is a narrow transition layer adjacent to the interface across which the surfactant concentration varies rapidly. Accurately resolving the layer is a significant challenge for traditional numerical methods but is essential to evaluate the exchange of surfactant between the interface and bulk flow. Previous studies have employed artificially small *Pe* or finely adapted grids in specific static geometries. The work described here uses the slenderness of the layer to develop a fast and accurate 'hybrid' or multiscale numerical method that incorporates a separate, singular perturbation analysis of the dynamics in the transition layer into a full numerical solution of the interfacial free boundary problem. A key to the success of this formulation is that highly accurate boundary integral or boundary element methods can readily be adapted to solve the full moving boundary problem, including soluble surfactant. Without the special large *Pe* treatment proposed here these methods do not easily apply.

The difficulties associated with computing interfacial flow with soluble surfactant were avoided in the study of [30] by specifying the computationally tractable but less physically realizable limit $Pe \ll 1$. Other numerical studies of soluble surfactant dynamics involving simple geometries or finely adapted three dimensional meshes for deformed interfaces are [29,31–36]. Ghadiali et al. [37] implemented a dual reciprocity boundary element method to solve for the steady state advection–diffusion of bulk surfactant. This has some features in common with the method proposed here, in that a boundary (element) method is used to solve the Stokes equations, while the bulk surfactant concentration is solved on internal nodes that do not have to be re-meshed as the boundary changes shape during iteration, as is required by other techniques (e.g. finite-element and finite difference methods). However, the method does require more internal nodes to be placed in positions of large concentration gradients, which can be expensive for realistic *Pe* values, and it is limited to steady state problems.

Recently, front tracking [36,38], diffuse interface [39], and volume of fluid [40] numerical methods have been designed to treat the effect of soluble surfactant in various examples of interfacial flow. But without adaptive or very fine meshes near the moving interface, these methods are limited to artificially small *Pe* due to the separation of spatial scales in the narrow transition layer and the need to accurately resolve it. In the context of mixing of miscible fluids, the study [41] combines front tracking with asymptotic treatment of the diffusion of mass across a near-discontinuity in density in the small diffusion limit.

In this paper we develop an accurate and efficient hybrid numerical algorithm, based on a boundary integral simulation of free surface Stokes flow. The hybrid method has the same advantages as the dual reciprocity method of [37], but applies to the simulation of time-dependent flow, and computes efficiently at arbitrarily large values of *Pe* without the need to introduce additional node points in regions of large gradient of bulk surfactant concentration. We implement and test the method in the case of a single, inviscid bubble that is stretched by an imposed linear strain or shear in 2D Stokes flow, although the hybrid method itself applies, with modifications, to more general flow in 3D and to multiple drops or bubbles.

The accuracy and efficiency of the hybrid method is assessed by comparison with a more 'traditional' numerical approach that uses finite differences on a curvilinear coordinate system exterior to the bubble, without the separate transition layer reduction.

The choice of underlying flow solver for the velocity, pressure, and surface concentration of surfactant used in both the hybrid and traditional methods is a boundary integral method based on a complex variable, conformal mapping representation of 2D Stokes flow. As explained below, this choice facilitates a traditional method that is in fact relatively efficient among finite difference methods and permits sufficient mesh refinement that it can compute well at *Pe* sufficiently large,

up to $Pe \simeq 10^4$, to facilitate a thorough test and comparison with the hybrid method. In particular, the traditional method features a novel, fast calculation of the fluid velocity in the region exterior to the bubble, without which the method would be prohibitively expensive.

The rest of this paper is organized as follows: The governing equations are presented in dimensionless form in Section 2. In Section 3 equations for the bulk and surface concentrations of surfactant are derived, based on a singular perturbation analysis in the large bulk Peclet number limit. The derivation in Section 3 is general, and the resulting equations describe surfactant dynamics at large Pe for interfaces in 3D Stokes flow with soluble surfactant. The boundary integral formulation of the equations governing fluid flow and interfacial surfactant concentration is given in Section 4. The hybrid numerical method is presented in Section 5 and the traditional method is presented in Section 6. Numerical results are given in Section 7, and concluding remarks are in Section 8. An asymptotic solution used in the validation of the hybrid method is derived in Appendix.

2. Governing equations

In this section we present the governing equations in nondimensional form following the formulation in [42]. Consider an inviscid bubble placed in two dimensional, incompressible slow viscous flow. The exterior fluid has viscosity μ and the same density as the interior fluid, so that the bubble is neutrally buoyant and gravitational effects are ignored. The pressure p_i of the inviscid interior fluid is constant in space, and without loss of generality is chosen to be zero. As a consequence of this choice, the pressure at infinity $p_\infty(t)$ is generally nonzero and time-dependent. The unbounded exterior region of fluid is denoted by Ω, while the fluid interface between the bubble and exterior bulk fluid is denoted by S. We follow the convention that the unit normal vector $\mathbf{n}$ on S points into Ω, and the unit tangent vector $\mathbf{t}$ on S points in the clockwise direction.

We take the zero Reynolds number limit, in which the nondimensional governing equations for the flow are the Stokes equations

$$\nabla^2\mathbf{u} = \nabla p, \qquad \nabla\cdot\mathbf{u} = 0, \quad \mathbf{x}\in\Omega, \tag{1}$$

where $\mathbf{u} = \mathbf{u}(x,y)$ is the fluid velocity and $p = p(x,y)$ is the pressure in Cartesian coordinates (x,y). All lengths are nondimensionalized by the radius a of the equivalent, undisturbed circular bubble, and with σ_0 as the interfacial surface tension in the absence of surfactant the velocity is made nondimensional by the capillary scale $U = \sigma_0/\mu$. Time and pressure are nondimensionalized by a/U and σ_0/a.

On the interface S we impose the kinematic condition that the normal velocity u_n at a point on the boundary equals the normal velocity of the fluid there, i.e.

$$u_n = \mathbf{u}\cdot\mathbf{n}, \tag{2}$$

while the stress-balance at the interface is

$$-p\mathbf{n} + 2\mathbf{e}\cdot\mathbf{n} = \sigma(\kappa_1+\kappa_2)\mathbf{n} - \nabla_s\sigma. \tag{3}$$

Here $\mathbf{e}$ is the rate-of-strain tensor, $e_{ij} = \frac{1}{2}(\partial_{x_j}u_i + \partial_{x_i}u_j)$, κ_i $(i=1,2)$ are the principal curvatures of S and $\nabla_s = \boldsymbol{\nabla} - \mathbf{n}(\mathbf{n}\cdot\boldsymbol{\nabla})$ is the surface gradient. The quantity σ in Eq. (3) is the surface tension, which depends on the adsorbed or surface concentration of surfactant Γ. The presence of surfactant generally acts to reduce surface tension, and a specific choice for the equation of state is the Langmuir equation

$$\sigma = 1 + E\ln(1-\Gamma), \tag{4}$$

which models a nonlinear dependence of σ on Γ. The surface tension has been made nondimensional by its value σ_0 for a clean or surfactant-free interface, the surface surfactant concentration has been made nondimensional by its maximum monolayer packing concentration Γ_∞, and $E = RT\Gamma_\infty/\sigma_0$ is the elasticity number, which is a dimensionless measure of the sensitivity of surface tension to adsorbed surfactant concentration. In practice, the surface tension has a strictly positive lower bound σ_{th} that occurs at some threshold value of $\Gamma < 1$.

When the adsorbed surfactant concentration Γ varies from point to point on S there is a spatial gradient of the surface tension that is represented in the stress-balance relation (3) by $\nabla_s\sigma$ and which is referred to as the Marangoni stress. Many of the important features and novel dynamics of surfactant-laden flows are in some way attributable to Marangoni stress, but an exception is discussed in [43].

Our focus is on surfactant that is soluble or dissolved in the bulk flow away from an interface, where it is transported as a passive scalar. Its concentration C, which is made nondimensional by a constant reference value at infinity C_∞, satisfies the advection–diffusion equation

$$\frac{\partial C}{\partial t} + \mathbf{u}\cdot\nabla C = \frac{1}{Pe}\nabla^2 C, \quad \mathbf{x}\in\Omega, \tag{5}$$

where Pe is the bulk Peclet number $Pe = Ua/D$, which is the ratio of advective to diffusive transport effects in the bulk, and D is the diffusivity of dissolved surfactant.

The evolution of surfactant that is adsorbed on the interface S also satisfies an advection–diffusion equation, which was derived for a general parametric representation of the interface $\mathbf{x} = \mathbf{X}(\xi,t)$ in [44], and is

$$\left.\frac{\partial \Gamma}{\partial t}\right|_{\xi} - \left.\frac{\partial \mathbf{X}}{\partial t}\right|_{\xi} \cdot \nabla_s \Gamma + \nabla_s \cdot (\Gamma \mathbf{u}_s) + \Gamma(\kappa_1 + \kappa_2) u_n = \frac{1}{Pe_s} \nabla_s^2 \Gamma + J\mathbf{n} \cdot \nabla C|_S. \tag{6}$$

Here, $\mathbf{u}_s = \mathbf{u} - \mathbf{n}(\mathbf{u} \cdot \mathbf{n})$ is the tangential fluid velocity on S, $u_n = \mathbf{u} \cdot \mathbf{n}$ is the normal component of the fluid velocity at the interface per (2), and $Pe_s = Ua/D_s$ is the surface Peclet number for surface diffusion of adsorbed surfactant on S. The surface gradient operator ∇_s and principal curvatures κ_i $(i = 1, 2)$ are as introduced at Eq. (3). On the left hand side of Eq. (6) the first two terms together ensure that if the interface moves then the time derivative of Γ is taken at a point on S that moves in the direction normal to the interface, while the next two terms account for the change in surfactant concentration due to advective flux along the interface and due to change in interface area caused by motion along its normal. The first term on the right hand side represents the change in Γ due to surface diffusion, which is usually negligible since typically $Pe_s \gg 1$, unless large surface gradients of adsorbed surfactant develop. The last term on the right hand side, $J\mathbf{n} \cdot \nabla C|_S$, accounts for the exchange or transfer of surfactant between its dissolved form in the bulk flow immediately adjacent to S (the sublayer region) and its adsorbed form on S, and $J = DC_\infty / U\Gamma_\infty$ is a transfer coefficient that measures the efficiency of this process.

Exchange of surfactant between the bulk phase and interface is a two step process [45]. In the bulk, surfactant is transported relative to material particles on the interface by diffusion, while exchange between the sublayer and interface occurs via adsorption–desorption kinetics. The net fluxes of the two steps are equal on S and are given by

$$j = Bi(K(1 - \Gamma)C|_S - \Gamma) = J\mathbf{n} \cdot \nabla C|_S, \tag{7}$$

where the second term is the net kinetic flux onto S, i.e. adsorption minus desorption, as described by a Langmuir-type kinetic rate expression. Here, the dimensionless parameter K is defined by $K = \kappa_a C_\infty / \kappa_d$, where the dimensional kinetic rate constants are κ_a for adsorption and κ_d for desorption, so that K is the ratio of the dissolved bulk surfactant concentration at infinity to the kinetic rate ratio or surface activity κ_d/κ_a. The Biot number is $Bi = a\kappa_d/U$, which is the ratio of the time scale a/U of capillary flow to the time scale for kinetic desorption. Since it occurs widely in applications, we consider the diffusion-controlled regime, i.e. the limit $Bi \to \infty$, in which the flow rate is much less than the adsorption–desorption kinetic rates, so that the surface exchange kinetics are effectively in equilibrium. In this case, (7) implies that

$$C|_S = \frac{\Gamma}{K(1 - \Gamma)} \quad \text{on } S, \tag{8}$$

which is the equilibrium adsorption relation of the Langmuir isotherm.

We note that the hybrid algorithm developed here for the large Peclet number limit, $Pe \to \infty$, is not confined to the diffusion-controlled regime. At finite arbitrary Biot number, the Dirichlet boundary condition for C of (8) is simply replaced by the mixed boundary condition of (7)

$$J\mathbf{n} \cdot \nabla C|_S = Bi(K(1 - \Gamma)C|_S - \Gamma).$$

In this study, the separation of time scales is such that the rate of bulk surfactant diffusion (D/a^2) is much less than the flow rate (U/a) since the Peclet number Pe is large, and the flow rate is much less than the surface kinetic rates since the Biot number Bi is large.

We assume that the bulk surfactant concentration approaches a constant reference value in the far-field and that the initial distribution of C is spatially uniform and in equilibrium with this, so that

$$C(\mathbf{x}, 0) = 1 \quad \text{for } \mathbf{x} \in \Omega, \qquad C \to 1 \quad \text{as } |\mathbf{x}| \to \infty. \tag{9}$$

If the initial configuration is in equilibrium everywhere, then the initial bubble shape is spherical and from (8) the initial surface concentration of surfactant is $\Gamma(\mathbf{x}, 0) = K/(1 + K)$.

The boundary condition at infinity corresponding to an arbitrary linear imposed flow is

$$\mathbf{u} = \begin{pmatrix} Q & B - \frac{G}{2} \\ B + \frac{G}{2} & -Q \end{pmatrix} \cdot \mathbf{x} + O(|\mathbf{x}|^{-2}) \quad \text{as } |\mathbf{x}| \to \infty. \tag{10}$$

Here $Q = a\alpha_\infty/U$, $B = a\beta_\infty/U$, and $G = a\omega_\infty/U$ are dimensionless, where Q and B characterize the strain rate of the imposed flow and $G\mathbf{e}_3$ is its vorticity. Two specific examples of a linear far-field flow that we use here are:

(i) *Pure Strain or Hyperbolic Flow*
When $B = G = 0$, the dimensionless far-field boundary condition is

$$\mathbf{u} = Q(x_1, -x_2) + O(|\mathbf{x}|^{-2}) \quad \text{as } |\mathbf{x}| \to \infty, \tag{11}$$

where Q is the capillary number or dimensionless strain rate.

(ii) *Simple Shear*
A simple shear flow is given by setting $Q = 0$ and $G = -2B \neq 0$, for which the boundary condition at infinity is

$$\mathbf{u} = -G(x_2, 0) + O(|\mathbf{x}|^{-2}) \quad \text{as } |\mathbf{x}| \to \infty. \tag{12}$$

3. The large bulk Peclet number limit

When the bulk Peclet number Pe is large a narrow transition layer in the bulk surfactant concentration C can develop adjacent to the interface. The layer has spatial width of order $Pe^{-1/2}$ in which the normal gradient of C is large. In the low Reynolds number limit there is no mechanism to support a similar transition layer in the fluid velocity and pressure.

To analyze the dynamics within the transition layer it is convenient to introduce an intrinsic or surface-fitted orthogonal curvilinear coordinate system (ξ_1, ξ_2, n) that is attached to the moving interface S for all time. Here the ξ_1 and ξ_2-directions are aligned with the principal directions of curvature and n is distance along the normal measured from S. The transformation between Eulerian coordinates $\mathbf{x}$ and intrinsic coordinates is uniquely invertible sufficiently close to S provided S is smooth. Analysis based on intrinsic coordinates attached to a moving surface has been used before. For example, Matalon et al. [46] give details of an arbitrary transformation of this type in 3D with application to combustion waves in the flamelet regime, while Yao and Stewart [47] have used a 2D version in the context of an evolving detonation front.

Here we review the transformation of the material derivative, and quote results for other operators. The origin of the Eulerian and intrinsic coordinate systems are O and O', respectively, and the position vector $\mathbf{x}$ of a point P in space relative to O is written in the two coordinate systems as

$$\mathbf{x} = \mathbf{X}(\xi_1, \xi_2, t) + n\mathbf{n}(\xi_1, \xi_2, t), \tag{13}$$

where $\mathbf{X}$ is the position vector relative to O of the projection of P onto S in the direction of the unit normal $\mathbf{n}$, so that S has equation $\mathbf{x} = \mathbf{X}(\xi_1, \xi_2, t)$. Since ξ_1 and ξ_2 are principal directions on S they define an orthogonal coordinate system on the surface, and the unit vectors $\mathbf{e}_i$ $(i = 1, 2)$ tangential to S in the directions of increasing ξ_i are $\mathbf{e}_i = \frac{1}{a_i}\frac{\partial \mathbf{X}}{\partial \xi_i}$ where $a_i = |\frac{\partial \mathbf{X}}{\partial \xi_i}|$. With the usual convention, the unit normal field is $\mathbf{n} = \mathbf{e}_1 \times \mathbf{e}_2$, and since the ξ_i are principal directions Rodrigues' formula implies that $\frac{\partial \mathbf{n}}{\partial \xi_i} = \kappa_i \frac{\partial \mathbf{X}}{\partial \xi_i}$ where the κ_i are the principal curvatures of S. The change in $\mathbf{x}$ corresponding to increments in the intrinsic coordinates with time fixed is therefore

$$\begin{aligned} &d\mathbf{x} = l_1 d\xi_1 \mathbf{e}_1 + l_2 d\xi_2 \mathbf{e}_2 + dn\mathbf{n} \\ &\text{where} \quad l_i = a_i(1 + n\kappa_i) \quad (i = 1, 2). \end{aligned} \tag{14}$$

This convention for $\mathbf{n}$ implies that, for the curve of a normal section of S with a plane containing $\mathbf{n}$ and $\mathbf{e}_i$, the curvature κ_i is positive when the curve is convex on the side to which $\mathbf{n}$ points, and is negative otherwise.

With P fixed relative to O, the time derivative in the Eulerian frame transforms as

$$\frac{\partial}{\partial t} \mapsto \frac{\partial}{\partial t} + \mathbf{q} \cdot \nabla_t + \frac{\partial n}{\partial t}\frac{\partial}{\partial n}. \tag{15}$$

Here ∂_t on the right hand side is in the moving frame, i.e. with intrinsic coordinates fixed,

$$\nabla_t = \frac{1}{l_1}\frac{\partial}{\partial \xi_1}\mathbf{e}_1 + \frac{1}{l_2}\frac{\partial}{\partial \xi_2}\mathbf{e}_2$$

is the projection of the gradient onto the tangent plane at P, and

$$\mathbf{q} = l_1 \frac{\partial \xi_1}{\partial t}\mathbf{e}_1 + l_2 \frac{\partial \xi_2}{\partial t}\mathbf{e}_2,$$

so that $\mathbf{q}$ is the velocity of P relative to O' projected onto the tangent plane at P. Since P is fixed relative to O, this is also $\mathbf{q} = -\mathbf{U}_s$ where $\mathbf{U}_s$ is the velocity of O' relative to O projected onto the tangent plane at P. Also, $-\frac{\partial n}{\partial t}$ is the normal speed of the surface S relative to O in the direction of $\mathbf{n}$, which was written earlier in the kinematic condition (2) as u_n.

The fluid velocity $\mathbf{u}$ at an arbitrary point P in the Eulerian frame is written in terms of its projection onto the tangent plane $\mathbf{u}_t$ and its component in the normal direction u_p as $\mathbf{u} = \mathbf{u}_t + u_p\mathbf{n}$. The gradient operator is written similarly as $\nabla = \nabla_t + \mathbf{n}\frac{\partial}{\partial n}$, so that $\mathbf{u} \cdot \nabla = \mathbf{u}_t \cdot \nabla_t + u_p \frac{\partial}{\partial n}$. As $n \to 0$ and S is approached the surface quantities are recovered, so that with the same notation as in Eqs. (2) and (6), $\mathbf{u}_t \to \mathbf{u}_s$, $u_p \to u_n$ and $\nabla_t \to \nabla_s$. Then from Eq. (15) the material derivative transforms as

$$\frac{D}{Dt} \mapsto \frac{\partial}{\partial t} + \mathbf{v}_t \cdot \nabla_t + v_p \frac{\partial}{\partial n}$$

where $\mathbf{v}_t = \mathbf{u}_t - \mathbf{U}_s$ is the fluid velocity relative to O' projected onto the tangent plane at P and $v_p = u_p - u_n$ is the normal component of the fluid velocity relative to S.

In the interface-attached intrinsic frame, Eq. (5) for the transport of surfactant in the bulk flow is therefore

$$\frac{\partial C}{\partial t} + \mathbf{v}_t \cdot \nabla_t C + v_p \frac{\partial C}{\partial n} = \epsilon^2 \nabla_s^2 C, \tag{16}$$

where $\epsilon = Pe^{-1/2}$ and the Laplacian is expressed in intrinsic coordinates. In the limit of large Pe, i.e. small ϵ, the bulk surfactant concentration C in the narrow transition layer adjacent to S depends on a local normal coordinate N, where $n = \epsilon N$ and $N = O(1)$ as $\epsilon \to 0$. While $C = C(\xi_1, \xi_2, N, t; \epsilon)$ within the layer, there is no mechanism available to support a similar separation of spatial scales for the fluid velocity, so that $\mathbf{v} = \mathbf{v}_t + v_p\mathbf{n} = \mathbf{v}(\xi_1, \xi_2, n, t; \epsilon)$.

An approximate equation for the evolution of C within the layer is given by keeping only the leading terms in an expansion for small ϵ. In this approximation, the tangential velocity $\mathbf{v}_t$ is replaced by its value on S,

$$\mathbf{v}_s = \mathbf{u}_s - \mathbf{U}_s \tag{17}$$

which is of order $O(1)$ except, for example, near stagnation points on the surface, and ∇_t is replaced by ∇_s. Since S is a fluid interface, the kinematic condition implies that v_p vanishes on S, so that it is replaced by the first nonzero term of its Taylor expansion, $\epsilon N \partial_n v_p|_s$ where the normal derivative $\partial_n v_p|_s$ is evaluated on S. The small $O(\epsilon)$ estimate in size of this coefficient in Eq. (16) multiplies the normal gradient of C, which is approximated by $(1/\epsilon)\partial_N C(\xi_1, \xi_2, N, t; 0)$. In a similar way, the small diffusion coefficient of Eq. (16) is magnified by the Laplacian of C within the layer, so that the right hand side of (16) is approximated by $\partial_N^2 C(\xi_1, \xi_2, N, t; 0)$. The reduced equation that results for the evolution of a first approximation to C within the layer is therefore

$$\frac{\partial C}{\partial t} + \mathbf{v}_s \cdot \nabla_s C + \left.\frac{\partial v_p}{\partial n}\right|_s N \frac{\partial C}{\partial N} = \frac{\partial^2 C}{\partial N^2}. \tag{18}$$

Consideration of higher order terms in the expansion implies that the error in approximating C by the solution of this equation is of order $O(\epsilon)$ as $\epsilon \to 0$.

The large Pe limit implies that outside the transition layer $(\partial_t + \mathbf{u} \cdot \nabla)C = 0$ to within $O(\epsilon)$, so that to this order C is constant on particle paths. The initial condition of (9), which holds for all $\mathbf{x}$ then implies that $C \equiv 1$ outside the transition layer for all time, so that (18) has initial, boundary and matching conditions

$$\begin{aligned} &C(\xi_1, \xi_2, N, 0) = 1, \quad C|_{N=0} = \frac{\Gamma}{K(1-\Gamma)}, \\ &C(\xi_1, \xi_2, N, t) \to 1 \quad \text{as } N \to \infty, \ t > 0. \end{aligned} \tag{19}$$

At a first glance, the coefficient $\partial_n v_p|_s$ in Eq. (18) appears to require the evaluation of off-surface data to compute the normal derivative. However, from the incompressibility condition $\nabla \cdot \mathbf{u} = 0$ written in the orthogonal curvilinear, intrinsic frame

$$\frac{1}{a_1 a_2}\left(\frac{\partial}{\partial \xi_1}(a_2(1+n\kappa_2)u_1)) + \frac{\partial}{\partial \xi_2}(a_1(1+n\kappa_1)u_2)\right) + \frac{\partial}{\partial n}((1+n\kappa_1)(1+n\kappa_2)u_p) = 0,$$

where the tangential velocity is written in terms of its components as $\mathbf{u}_t = u_1\mathbf{e}_1 + u_2\mathbf{e}_2$ and $u_p = v_p + u_n$. When the incompressibility condition is evaluated in the limit as $n \to 0$, the first two terms tend to the surface divergence $\nabla_s \cdot \mathbf{u}_s$, and since the normal speed u_n of the surface is independent of n, so that $\partial_n u_p = \partial_n v_p$, the condition implies that

$$\left.\frac{\partial v_p}{\partial n}\right|_S = -(\kappa_1 + \kappa_2)u_n - \nabla_s \cdot \mathbf{u}_s, \tag{20}$$

where the right hand side contains surface data alone.

The transfer coefficient J in the bulk-interface exchange term $J\mathbf{n} \cdot \nabla C|_S$ is rescaled by putting $J = \epsilon J_0$ where $J_0 = O(1)$ so that in Eq. (6) for conservation of adsorbed surfactant the exchange term remains $O(1)$ when expressed in terms of the rescaled coordinate N. The equation becomes

$$\left.\frac{\partial \Gamma}{\partial t}\right|_\xi - \left.\frac{\partial \mathbf{X}}{\partial t}\right|_\xi \cdot \nabla_s \Gamma + \nabla_s \cdot (\Gamma \mathbf{u}_s) + \Gamma(\kappa_1 + \kappa_2)u_n = \frac{1}{Pe_s}\nabla_s^2 \Gamma + J_0 \left.\frac{\partial C}{\partial N}\right|_S. \tag{21}$$

The initial boundary value problem (18) and (19) for C within the transition layer and the rescaled bulk-interface exchange term of (21) have been constructed by a (formal) leading order, singular perturbation rescaling of the full equations in the limit $Pe \to \infty$. As a result, the expansion parameter Pe does not appear in the rescaled model.

4. Boundary integral formulation

A complex variable representation is used to provide a boundary integral formulation of the governing equations which is based on the work of Tanveer and Vasconcelos [48], Antanovskii [49], and Siegel [42]. It includes the effects of soluble surfactant assuming that the bulk-interface exchange term $J\mathbf{n} \cdot \nabla C|_S$ is known via separate computation. We briefly summarize the formulation of [48], including the necessary modifications of [42] to account for the presence of surfactant. These references contain more complete details of the derivation.

4.1. Complex variable representation of Stokes flow

We introduce a stream function $\psi(x, y)$ and a stress function $\phi(x, y)$ which satisfy [50]

$$\nabla^2 \psi = -\omega, \quad \nabla^2 \phi = p,$$

where ω is the fluid vorticity. The Stokes Eq. (1) imply that ϕ and ψ obey the biharmonic equation

$$\nabla^4\phi = \nabla^4\psi = 0.$$

The complex stress-stream function is defined by $W(z,\bar{z}) = \phi(x,y) + i\psi(x,y)$, where $z = x + iy$ and the bar denotes complex conjugate, for which a Goursat representation of solutions of the biharmonic equation implies that $W(z,\bar{z})$ can be written as (see, e.g. [51])

$$W(z,\bar{z}) = \bar{z}f(z) + g(z),$$

where f and g are analytic functions in the fluid region Ω. Nondimensional physical quantities can be expressed in terms of f and g as (see, e.g. [52])

$$p - i\omega = 4f'(z), \tag{22}$$

$$u_1 + iu_2 = -f(z) + z\bar{f}'(\bar{z}) + \bar{g}'(\bar{z}), \tag{23}$$

$$e_{11} + ie_{12} = z\bar{f}''(\bar{z}) + \bar{g}''(\bar{z}), \tag{24}$$

where $\bar{f}$ denotes the (analytically continued) conjugate function $\bar{f}(z) = \overline{f(\bar{z})}$ and a prime denotes the derivative. Here $u_1 + iu_2$ is a complex velocity, $e_{11} + ie_{12}$ is a complex rate-of-strain function, and the dependence on time has temporarily been suppressed.

We introduce the conformal map $z(\zeta,t)$ which takes the unit disc $|\zeta| < 1$ in the ζ-plane into the fluid region Ω of the z-plane. The map takes the form

$$z(\zeta,t) = \frac{a(t)}{\zeta} + h(\zeta,t), \tag{25}$$

where $h(\zeta,t)$ is analytic, $h(0,t) = 0$ without loss of generality, and $z_\zeta(\zeta,t) \neq 0$ in $0 \leqslant |\zeta| \leqslant 1$ over some nonzero time interval. The extra degree of freedom allowed by the Riemann mapping theorem permits $a(t)$ to be chosen real and negative.

The boundary conditions in the far-field $z \to \infty$ determine the behavior of $f(z(\zeta,t),t)$ and $\frac{dg}{dz}(z(\zeta,t),t)$ as $\zeta \to 0$. Since $p \to p_\infty(t)$ and $\omega \to G$ in this limit, from (22) and (25),

$$f(z(\zeta,t),t) \sim \frac{a(t)(p_\infty(t) - iG)}{4\zeta} + C(t) + O(\zeta), \tag{26}$$

as $\zeta \to 0$, while (10), (23), and (26) imply that

$$\frac{dg}{dz}(z(\zeta,t),t) \sim \frac{a(t)(Q - iB)}{\zeta} + \overline{C(t)} + O(\zeta^2) \tag{27}$$

as $\zeta \to 0$. The nondimensional far-field pressure $p_\infty(t)$ and the function $C(t)$ are to be determined. We recall from (10) that there is no translational velocity in the far-field, and we assume that the bubble interior is free of mass sources and therefore has constant volume.

Eqs. (22)–(24) are used to write the boundary conditions on the bubble surface in terms of $f(z)$ and $g(z)$. The outward unit normal on the bubble surface $\mathbf{n}$ is written in complex form as

$$N = n_1 + in_2 = iz_s = -\zeta\frac{z_\zeta}{|z_\zeta|} = i\frac{z_\nu}{|z_\nu|}, \tag{28}$$

where n_1 and n_2 are the x and y components of $\mathbf{n}$, s is arclength traversed in the clockwise direction, and $\zeta = e^{i\nu}$ on the unit circle. When (22) and (24) are substituted into the stress-balance equation (3) an integration with respect to s gives

$$f(z,t) + z\bar{f}'(\bar{z},t) + \bar{g}'(\bar{z},t) = -\frac{i}{2}\sigma(\Gamma(s,t))z_s \tag{29}$$

on the bubble surface $|\zeta| = 1$, where we emphasize the dependence of the surface tension σ on the adsorbed surfactant concentration $\Gamma(s,t)$. Some arbitrariness in the specification of the functions f and g has also been used to set to zero a function of time that results from the integration. A formula for the velocity on the bubble surface follows on eliminating g between (23) and (29) to obtain

$$u_1 + iu_2 = -\frac{i}{2}\sigma(\Gamma(s,t))z_s - 2f(z,t). \tag{30}$$

A relation between the map $z(\zeta,t)$ and the Goursat function f in $|\zeta| < 1$ follows from the kinematic condition (2) written in complex form together with (30) and (28) followed by application of the Poisson integral formula to extend the relation away from the bubble surface, with the result that [48]

$$z_t + 2f(\zeta,t) = \zeta[I(\zeta,t) + iD]z_\zeta, \tag{31}$$

where

$$I(\zeta,t) = \frac{1}{4\pi i}\oint_{|\zeta'|=1}\left[\frac{\zeta' + \zeta}{\zeta' - \zeta}\right]\frac{\sigma(\Gamma(z(\zeta',t),t))}{|z_\zeta(\zeta',t)|}\frac{d\zeta'}{\zeta'}, \tag{32}$$

and $f(\zeta,t)$ denotes $f(z(\zeta,t),t)$. Note that $I(\zeta,t)$ depends on the adsorbed surfactant concentration at $z(\zeta,t)$ via the term $\sigma(\Gamma(z(\zeta,t),t))$ in the integrand. The constant D is determined by expanding (31) as $\zeta \to 0$ and equating singular terms to give

$$D = \frac{G}{2} \quad \text{and} \quad p_\infty(t) = -2\left[I(0,t) + \frac{\dot{a}}{a}\right]. \tag{33}$$

Eq. (31) is not practical for evolving the map $z(\zeta,t)$, since the Goursat function $f(z,t)$ is as yet unknown. Evolution equations for the map parameters are derived in Section 4.2.

A relation for $\frac{dg}{dz}(z(\zeta,t),t)$ is found on eliminating f between (29) and (31) and using (28), with the result that

$$\frac{dg}{dz}(z(\zeta,t),t)) = \frac{\bar{z}(\zeta^{-1},t)}{2}\left\{\frac{z_{\zeta t}(\zeta,t)}{z_\zeta(\zeta,t)} - \zeta I_\zeta(\zeta,t) - \left[1 + \frac{\zeta z_{\zeta\zeta}(\zeta,t)}{z_\zeta(\zeta,t)}\right][I(\zeta,t) + iD]\right\} + \frac{\bar{z}_\zeta(\zeta^{-1},t)}{2\zeta}[I(\zeta,t) + iD] + \frac{\bar{z}_t(\zeta^{-1},t)}{2}, \tag{34}$$

which is valid on $|\zeta| = 1$ and is extended off the unit circle by analytic continuation. The requirement that the right hand side of (34) is analytic in $|\zeta| < 1$ except for a known pole at $\zeta = 0$ (see (27)) determines the time evolution of the map $z(\zeta,t)$, as seen in Section 4.2.

The complex variable formulation for conservation of adsorbed surfactant (6) is derived by combining the complex analogue of the vectors, dot products and derivatives that appear in it, i.e.

$$\begin{aligned} &\left.\frac{\partial \mathbf{X}}{\partial t}\right|_\xi \leftrightarrow \left.\frac{\partial z}{\partial t}\right|_v, \quad \nabla_s \leftrightarrow \frac{T}{|z_v|}\frac{\partial}{\partial v}, \quad \mathbf{u}_s \leftrightarrow \mathrm{Re}\{(u_1 + iu_2)\overline{T}\}T, \\ &\kappa \leftrightarrow -\frac{1}{|z_v|}\mathrm{Im}\left(\frac{z_{vv}}{z_v}\right), \quad u_n \leftrightarrow \mathrm{Re}\{(u_1 + iu_2)\overline{N}\}, \ \mathbf{n}\cdot\nabla C|_S \leftrightarrow -\frac{1}{|z_v|}\left.\frac{\partial C}{\partial r}\right|_{r=1} \end{aligned} \tag{35}$$

where $T = z_v/|z_v|$ is the clockwise oriented surface tangent and $C = C(r,v)$ is the concentration of dissolved surfactant at $z(\zeta = re^{iv},t)$. If we define

$$U(v,t) = (u_1 + iu_2)\frac{\bar{z}_v}{|z_v|} \tag{36}$$

then the complex form of (6) is

$$\frac{\partial \Gamma}{\partial t} - \mathrm{Re}\left(\frac{z_t}{z_v}\right)\Gamma_v + \frac{1}{|z_v|}\left\{\frac{\partial}{\partial v}(\mathrm{Re}(\Gamma U)) - \mathrm{Im}\left(\frac{z_{vv}}{z_v}\right)\mathrm{Im}(\Gamma U)\right\} = \frac{1}{Pe_s}\frac{1}{|z_v|}\frac{\partial}{\partial v}\left(\frac{\Gamma_v}{|z_v|}\right) - \frac{J}{|z_v|}\left.\frac{\partial C}{\partial r}\right|_{r=1}, \tag{37}$$

which holds on the interface $\zeta = e^{iv}$, where the time derivatives are taken with v fixed. This is the form that the equation takes in the traditional numerical method, while in the hybrid method the last, surfactant exchange, term is rewritten as $J_0\partial_N C|_S$ in the same way that the real form of the conservation law (6) becomes (21) in the large Pe limit.

Eq. (18) for conservation of bulk surfactant is transformed similarly. The tangential velocity of the origin of the intrinsic frame, O', is $\mathbf{U}_s = (\partial_t \mathbf{X}|_\xi \cdot \mathbf{t})\mathbf{t} \leftrightarrow \mathrm{Re}(z_t\overline{T})T$, (where O' is chosen to be the image of the point with $v = 0$) so that

$$\mathbf{v}_s = \mathbf{u}_s - \mathbf{U}_s \leftrightarrow \mathrm{Re}((u_1 + iu_2 - z_t)\overline{T})T$$

(cf. (17)). The relations (35) and (36) together with the complex form of $\partial_n v_p|_S$ constructed from (20) imply that (18) becomes

$$\frac{\partial C}{\partial t} + \mathrm{Re}\left(U - \frac{z_t\bar{z}_v}{|z_v|}\right)\frac{1}{|z_v|}\frac{\partial C}{\partial v} - \frac{1}{|z_v|}\left\{\frac{\partial}{\partial v}(\mathrm{Re}(U)) - \mathrm{Im}\left(\frac{z_{vv}}{z_v}\right)\mathrm{Im}(U)\right\}N\frac{\partial C}{\partial N} = \frac{\partial^2 C}{\partial N^2}. \tag{38}$$

This holds in the fluid region $N > 0$, where the time derivatives are taken with the intrinsic coordinates v and N fixed, and the initial and boundary conditions are given by (19).

4.2. Boundary integral equations

Following [48] we consider maps $z(\zeta,t)$ in which $h(\zeta,t)$ is a polynomial of degree N

$$z(\zeta,t) = \frac{a(t)}{\zeta} + \sum_{j=1}^{N} b_j(t)\zeta^j, \tag{39}$$

where the b_j's are complex coefficients. Here (39) is interpreted as the truncated Fourier series expansion of a discrete solution, although [42] shows (following [48]) that no higher powers of ζ are generated in a continuous solution for $N \geqslant 1$. Equations for the coefficients $a(t)$, $b_j(t)$ are obtained by enforcing the analyticity of the right hand side of (34) in $|\zeta| < 1$. Define the Taylor series coefficients $\widehat{I}_0(t), \widehat{I}_k(t)$ by

$$I(\zeta,t) + iD = \widehat{I}_0(t) + \sum_{k=1}^{\infty}\widehat{I}_k(t)\zeta^k, \tag{40}$$

where (see (32))

$$\widehat{I}_0 = \frac{1}{4\pi}\int_0^{2\pi} \frac{\sigma(v,t)}{|z_\zeta(e^{iv},t)|}\,dv + iD,$$
$$\widehat{I}_k = \frac{1}{2\pi}\int_0^{2\pi} \frac{\sigma(v,t)e^{-ikv}}{|z_\zeta(e^{iv},t)|}\,dv, \tag{41}$$

and we have written $\sigma(v,t) = \sigma(\Gamma(z(e^{iv},t),t))$.

Substitution of (39) and (41) into the right hand side of (34) leads to a Laurent series in ζ, and matching coefficients of the series from the right and left hand sides of this equation gives a system of ODE's for $a(t)$, $b_j(t)$. This system is written (following [48]) by defining the quantities c_k

$$c_{N+2} = a\bar{b}_N,$$
$$c_{N+1} = a\bar{b}_{N-1},$$
$$c_k = a\bar{b}_{k-2} - \sum_{j=1}^{N+1-k} jb_j\bar{b}_{k+j-1}, \quad 3 \leqslant k \leqslant N,$$
$$c_2 = -\sum_{j=1}^{N-1} jb_jb_{j+1},$$
$$c_1 = a^2 - \sum_{j=1}^{N} j|b_j|^2. \tag{42}$$

The ODE's then take the form

$$\dot{c_1} = 0,$$
$$\dot{c_k} = -(k-1)\sum_{j=0}^{N+2-k} \widehat{I}_j c_{k+j} + 2a^2(Q - iB)\delta_{k3}, \quad 3 \leqslant k \leqslant N+2. \tag{43}$$

An expression for the velocity on the interface is given by analytic continuation of (31) to $|\zeta| = 1$ by contour deformation, followed by elimination of $f(z)$ from (30), with the result that

$$u_1 + iu_2 = z_t - \zeta z_\zeta \mathcal{H}\left(\frac{\sigma}{|z_v|}\right), \tag{44}$$

where the Hilbert transform $\mathcal{H}$ is defined by

$$\mathcal{H}(h(v,t)) = \frac{1}{4\pi i} PV \int_0^{2\pi} h(v',t)\cot\frac{(v'-v)}{2}\,dv' \tag{45}$$

and *PV* denotes the Cauchy principal value.

Eqs. (37) and (42), (43) give the desired boundary integral formulation for the interface shape and surfactant concentration Γ when the exchange of surfactant between the bulk fluid and the interface, represented by the term $J\mathbf{n}\cdot\nabla C|_S$, is known by a separate computation of the problem for C. Alternative boundary integral formulations of Stokes flow such as those given in [9] can also be used as a basis for the hybrid method proposed here.

4.3. Pure strain and simple shear flows

In the case of an initially circular or elliptical bubble placed in either a pure strain or simple shear flow it can be shown from Eqs. (42) and (43) that the interface is described at times $t > 0$ by a conformal map of the truncated form

$$z(\zeta,t) = \frac{a(t)}{\zeta} + b(t)\zeta. \tag{46}$$

This holds when the flow is surfactant-free [48], when there is insoluble surfactant on the interface [42], or with soluble surfactant, as just seen in the development of Sections 4.1 and 4.2. In particular, it implies that the interface shape remains elliptical for all time, although the aspect ratio is influenced by the presence of surfactant and its solubility. This result also depends, as assumed at the outset, on the flow geometry being two dimensional and the interior bubble fluid being inviscid.

(i) *Pure Strain*

In a pure strain, $\mathbf{u} = Q(x_1, -x_2)$ where Q is the capillary number, per (11). Since the imposed flow has vorticity $G = 0$, (33) and (41) imply that $\widehat{I}_0$ is real. The map parameters $a(t)$ and $b(t)$ are also real, with $a(t) < 0$, and satisfy

$$\frac{d}{dt}(ab) = -2\widehat{I}_0 ab + 2Qa^2, \quad a(0) = -1, \;\; b(0) = 0, \tag{47}$$

with the area condition

$$a^2 - b^2 = 1. \tag{48}$$

The initial conditions of (47) are for a bubble that is initially circular.

(ii) *Simple shear*

In a simple shear flow, $\mathbf{u} = -G(x_2, 0)$ where G is the shear strength, per (12). Here $\widehat{I}_0$ and $b(t)$ are complex, while $a(t) < 0$, and the map parameters satisfy

$$\frac{d}{dt}(ab) = -2\widehat{I}_0 ab - iGab + iGa^2, \quad a(0) = -1, \;\; b(0) = 0, \tag{49}$$

with the area condition

$$a^2 - |b|^2 = 1. \tag{50}$$

With soluble surfactant, the motion of the interface is coupled to the bulk concentration C and the surface concentration Γ through the surface tension σ in the integral term $\widehat{I}_0$. We describe below an efficient method for solving the coupled equations in the physically representative limit of large bulk Peclet number *Pe*.

5. Hybrid numerical method

Our implementation of the hybrid method combines a fixed grid numerical solution of the boundary value problem (38) and (19) for dissolved surfactant C with simultaneous solution of the underlying problem for $\mathbf{u}$, p, and Γ. This has the advantage that there is no need to re-mesh the grid that is used to solve for C as the interface evolves, and since the diffusive term $\partial_N^2 C$ is $O(1)$ in the rescaled transition layer Eq. (38), there is no development of large concentration gradients that requires a large number of node points to resolve. The underlying flow solver for $\mathbf{u}$, p, and Γ described in Section 4 is spectrally accurate in space and second order in time, while the solution for the dissolved surfactant concentration C described below is second order accurate (in space and time). In principle higher order accuracy can be achieved.

To describe the method, the evolution equations, which are (37), with its last term rewritten as $J_0 \partial_n C|_S$, (38) and (43) (which simplifies to (47) and (48) for a pure strain and (49) and (50) for a simple shear) are written in the form

$$\begin{pmatrix} z \\ \Gamma \end{pmatrix}_t = \mathbf{F}\left(z, \Gamma, \frac{\partial C}{\partial N}\Big|_S\right), \tag{51}$$

$$C_t = G(z, \Gamma, C) + \frac{\partial^2 C}{\partial N^2}, \tag{52}$$

where $\mathbf{F}$ and G depend on the indicated variables and their derivatives. Note that, in terms of the parameterization by v in the ζ-plane and time t, $\mathbf{F} = \mathbf{F}(v, t)$ is defined on the bubble surface, while $G = G(v, N, t)$ is defined in the region exterior to the bubble. We assume that the bulk concentration C is initially in equilibrium with the far-field concentration, i.e. $C(v, N, t = 0) = 1$, and far from the interface we impose the boundary condition $C(v, N_m, t) = 1$. It is verified that the numerical results do not depend on the particular value of N_m. We introduce the discrete variables $v_i = 2\pi i/M$ for $i = 0, \ldots, M-1$ and $N_j = jN_m/(P-1)$ for $j = 0, \ldots, P-1$, with the notation $\mathbf{F}_i^n = \mathbf{F}(v_i, t^n)$ and $G_{ij}^n = G(v_i, N_j, t^n)$.

Second order accuracy in time is achieved by performing the time update of Eqs. (51) and (52) in two steps. First we compute the intermediate values $\tilde{z}_i^{n+1}, \tilde{\Gamma}_i^{n+1}$, and $\widetilde{C}_{ij}^{n+1}$ by a first order Euler method

$$\begin{pmatrix} \tilde{z}_i^{n+1} \\ \tilde{\Gamma}_i^{n+1} \end{pmatrix} = \begin{pmatrix} z_i^n \\ \Gamma_i^n \end{pmatrix} + \Delta t \mathbf{F}_i^n,$$

$$\widetilde{C}_{ij}^{n+1} = C_{ij}^n + \Delta t \left(G_{ij}^n + \frac{\widetilde{C}_{ij+1}^{n+1} + \widetilde{C}_{ij-1}^{n+1} - 2\widetilde{C}_{ij}^{n+1}}{(\Delta N)^2} \right). \tag{53}$$

where $C_{i0}^n = \frac{\Gamma_i^n}{K(1-\Gamma_i^n)}$ from the boundary condition (19). A second order accurate correction is calculated using a centered discretization

$$\begin{pmatrix} z_i^{n+1} \\ \Gamma_i^{n+1} \end{pmatrix} = \begin{pmatrix} z_i^n \\ \Gamma_i^n \end{pmatrix} + \frac{\Delta t}{2}\left(\mathbf{F}_i^n + \widetilde{\mathbf{F}}_i^{n+1} \right),$$

$$C_{ij}^{n+1} = C_{ij}^n + \frac{\Delta t}{2}\left(G_{ij}^n + \widetilde{G}_{ij}^{n+1} + \frac{C_{ij+1}^n + C_{ij-1}^n - 2C_{ij}^n}{(\Delta N)^2} + \frac{C_{ij+1}^{n+1} + C_{ij-1}^{n+1} - 2C_{ij}^{n+1}}{(\Delta N)^2} \right). \tag{54}$$

The discretizations (53) and (54) are semi-implicit, and the resulting tridiagonal linear systems are inverted by standard methods.

The right hand sides of (53) and (54) are evaluated at mesh points (v_i, N_j) as follows. We compute the derivatives of surface quantities, such as $z_v(v_i, t^n)$ and $\Gamma_v(v_i, t^n)$, using a discrete Fourier transform (DFT) and employ a centered, second order finite difference approximation for $C_v(v_i, N_j, t^n)$ (although we note that in principle all v derivatives can be computed

in Fourier space). A spectral filter with cutoff of $\epsilon_c = 10^{-14}$ is used to prevent amplification of round-off error when taking derivatives. We also need the normal derivative of the bulk surfactant concentration evaluated at the bubble surface, $\partial_N C|_S$, which is calculated using the second order, one-sided difference formula

$$\left[\frac{\partial C}{\partial N}\Big|_S\right]_i^n = \frac{-3C_{i,0}^n + 4C_{i,1}^n - C_{i,2}^n}{2\Delta N}. \tag{55}$$

The Taylor coefficients $\widehat{I}_k$ defined at (41) are needed to solve the ODEs (43) for the time evolution of the conformal map parameters, and are calculated via a DFT. The fluid velocity on the bubble surface is also calculated via a DFT and the relation

$$\mathcal{H}[h(v)] = \frac{1}{2}(h_+ - h_-), \tag{56}$$

where $h_+ = \sum_{k>0}\hat{h}_k e^{ikv}$ is a projection onto the positive wavenumber Fourier components of h, and $h_- = \sum_{k<0}\hat{h}_k e^{ikv}$ is a projection onto the negative wavenumber components. An expression for the time derivative $z_t(v_i, t^n)$ is required for the velocity calculation, and is obtained from the system of ODEs (43), while the normal derivative of the normal fluid velocity relative to the interface, $\partial_n v_p|_S$, is calculated from surface data by the relation (20).

The method generates the time update of the fluid velocity and surface concentration of surfactant in $O(M)$ operations, where M is the number of discretization points on the interface. Calculation of the bulk surfactant concentration requires $O(MP)$ operations, where P is the number of grid points normal to the interface. The operation count increases to $O(M^2P)$ for three dimensional flow. Knowledge of the bulk concentration C and its gradient $\nabla C|_S$ at the interface is sufficient for the time update of interface position and surface surfactant concentration in the transition layer equation.

We also require a solution to the advection equation $(\partial_t + \mathbf{u}\cdot\nabla)C = 0$ outside the transition layer, which provides a boundary or matching condition for the transition layer equation as $N \to \infty$. Generally, this requires $O(M^{d-1}P)$ operations for $M^{d-1}P$ points in the fluid region for d-dimensional flow. A coarse grid will often suffice, since large concentration gradients are not expected outside the transition layer. Semi-Lagrangian methods can also be used to track C in regions where it differs from the equilibrium value $C = 1$, which can further reduce the operation count. All calculations in this paper assume a spatially uniform state with $C = 1$ far from the interface.

6. Traditional numerical method

The hybrid method has been compared with a more traditional numerical approach, i.e. one that uses finite differences on a curvilinear coordinate system exterior to the bubble, without the separate transition layer reduction. However, due to separation of scales in the narrow transition layer and the need to accurately resolve the layer, the traditional algorithm is limited to values of Pe less than about 10^3 for reasonably fine meshes (e.g. 512×512 gridpoints in an annular fluid region with thickness of a few bubble radii). Our implementation of the traditional method features a novel fast calculation of the fluid velocity in the region exterior to the bubble.

The algorithm, which is simplest to describe using real variables and vector notation, makes use of the mapping

$$\mathbf{X}(r, v) = (x(r, v), y(r, v,)) = (\mathrm{Re}z(r, v), \mathrm{Im}z(r, v)) \tag{57}$$

from the unit disc $\zeta = re^{iv}$ for $0 \leqslant r \leqslant 1$ to the fluid region exterior to the bubble. The advection–diffusion equation (5) for dissolved surfactant C is expressed in terms of the orthogonal curvilinear coordinate system defined by the map. Introduce the unit vectors

$$\mathbf{e_r} = -\frac{1}{l_1}\frac{\partial \mathbf{X}}{\partial r}, \quad \mathbf{e}_v = \frac{1}{l_2}\frac{\partial \mathbf{X}}{\partial v}, \tag{58}$$

where the scale factors $l_1(r, v)$ and $l_2(r, v)$ are given by

$$l_1 = \left|\frac{\partial \mathbf{X}}{\partial r}\right|, \quad l_2 = \left|\frac{\partial \mathbf{X}}{\partial v}\right|. \tag{59}$$

The vector $\mathbf{e_r}$ is in the outward normal direction to the coordinate curve traced out by $\mathbf{X}(r, v)$ for fixed r, while $\mathbf{e}_v$ points in the (clockwise) tangential direction to this curve. We recall that

$$\nabla C = \left(-\frac{\mathbf{e_r}}{l_1}\frac{\partial}{\partial r} + \frac{\mathbf{e}_v}{l_2}\frac{\partial}{\partial v}\right)C, \tag{60}$$

$$\nabla^2 C = \frac{1}{l_1 l_2}\left(\frac{\partial}{\partial r}\frac{l_2}{l_1}\frac{\partial}{\partial r} + \frac{\partial}{\partial v}\frac{l_1}{l_2}\frac{\partial}{\partial v}\right)C. \tag{61}$$

The boundary integral solution of Eqs. (37) and (43) for the conformal map $z(\zeta, t)$ and surface concentration of surfactant $\Gamma(v, t)$ described in Section 4.2 is coupled to solution of the advection–diffusion equation for C in the annular region $0 < 1 - r_m \leqslant r \leqslant 1$.

Various discretizations of the governing equation for C have been considered, including upwind and centered differencing of the advection term, as well as explicit and implicit treatment of the diffusion term. An implicit ADI method [53] utilizing

upwind differencing for the advection terms in the equations for both C and Γ was found to be the most efficient. The ADI scheme is a two step method, and is implemented with first step

$$C_{ij}^{n+1/2} = C_{ij}^n + \frac{\Delta t}{2}\left\{\frac{w_{ij}^n}{Pe}\left[p_{ij+1/2}^n \delta_r C_{ij+1/2}^{n+1/2} - p_{ij-1/2}^n \delta_r C_{ij-1/2}^{n+1/2} + q_{i+1/2j}^n \delta_v C_{i+1/2j}^n - q_{i-1/2j}^n \delta_v C_{i-1/2j}^n\right] - \mathbf{u}\cdot\nabla C|_{ij}^n\right\}. \tag{62}$$

Here we have introduced the centered difference operators δ_r and δ_v,

$$\delta_r C_{ij+1/2}^n = \frac{C_{ij+1}^n - C_{ij}^n}{-\Delta r}, \quad \delta_v C_{i+1/2j}^n = \frac{C_{i+1j}^n - C_{ij}^n}{\Delta v}, \tag{63}$$

and

$$p_{ij+\frac{1}{2}}^n = \frac{1}{2}\left(\frac{l_2}{l_1}\Big|_{ij}^n + \frac{l_2}{l_1}\Big|_{ij+1}^n\right), \quad q_{i+\frac{1}{2}j}^n = \frac{1}{2}\left(\frac{l_1}{l_2}\Big|_{ij}^n + \frac{l_1}{l_2}\Big|_{i+1j}^n\right), \quad w_{ij}^n = \frac{1}{l_1 l_2}\Big|_{ij}^n. \tag{64}$$

The subscript (i,j) refers to the (v_i, r_j) gridpoint with $r_j = 1 - \frac{r_m j}{P-1}$ for $j = 0,\ldots,P-1$, and $\Delta v = v_{i+1} - v_i,\ \Delta r = r_{j+1} - r_j$. The second step of the ADI scheme is

$$C_{ij}^{n+1} = C_{ij}^{n+1/2} + \frac{\Delta t}{2}\left\{\frac{w_{ij}^{n+1/2}}{Pe}\left[p_{ij+1/2}^{n+1/2} \delta_r C_{ij+1/2}^{n+1/2} - p_{ij-1/2}^{n+1/2} \delta_r C_{ij-1/2}^{n+1/2} + q_{i+1/2j}^{n+1/2} \delta_v C_{i+1/2j}^{n+1} - q_{i-1/2j}^{n+1/2} \delta_v C_{i-1/2j}^{n+1}\right] - \mathbf{u}\cdot\nabla C|_{ij}^{n+1/2}\right\}, \tag{65}$$

and initial and boundary conditions are given by (19). The discretizations (62) and (65) lead to tridiagonal linear systems that are readily inverted by standard methods.

Calculation of the advection term $\mathbf{u}\cdot\nabla C$ requires the radial and tangential velocity components, which are given by

$$\begin{aligned} u^r &= \mathbf{u}\cdot\mathbf{e}_\mathbf{r} = -\frac{1}{l_1}\left(u_1\frac{\partial x}{\partial r} + u_2\frac{\partial y}{\partial r}\right), \\ u^v &= \mathbf{u}\cdot\mathbf{e}_v = \frac{1}{l_2}\left(u_1\frac{\partial x}{\partial v} + u_2\frac{\partial y}{\partial v}\right). \end{aligned} \tag{66}$$

The upwind difference scheme in the case $u^r|_{ij}^n > 0$ and $u^v|_{ij}^n > 0$ is

$$\mathbf{u}\cdot\nabla C|_{ij}^n = \frac{u^r}{l_1}\Big|_{ij}^n \delta_r^- C_{ij}^n + \frac{u^v}{l_2}\Big|_{ij}^n \delta_v^- C_{ij}^n, \tag{67}$$

where

$$\delta_r^- C_{ij}^n = \frac{C_{ij}^n - C_{ij-1}^n}{-\Delta r} \quad \text{and} \quad \delta_v^- C_{ij}^n = \frac{C_{ij}^n - C_{i-1j}^n}{\Delta v}. \tag{68}$$

If $u^r|_{ij}^n < 0$ or $u^v|_{ij}^n < 0$ the corresponding difference quotient in (67) is replaced by

$$\delta_r^+ C_{ij}^n = \frac{C_{ij+1}^n - C_{ij}^n}{-\Delta r} \quad \text{or} \quad \delta_v^+ C_{ij}^n = \frac{C_{i+1j}^n - C_{ij}^n}{\Delta v}, \tag{69}$$

respectively. The derivatives $\frac{\partial \mathbf{x}}{\partial r}(v_i, r_j)$ and $\frac{\partial \mathbf{x}}{\partial v}(v_i, r_j)$ at (58) and (59), which define the unit vectors $\mathbf{e}_\mathbf{r},\ \mathbf{e}_v$ and scale factors $l_1,\ l_2$ are calculated at the $(v_i,\ r_j)$ gridpoint with the aid of the relations

$$z_r(r_j e^{iv_i}) = z_\zeta(r_j e^{iv_i})e^{iv_i}, \quad z_v(r_j e^{iv_i}) = z_\zeta(r_j e^{iv_i}) i r_j e^{iv_i}, \tag{70}$$

where z_ζ is determined by differentiation of (39).

Our implementation of the traditional method is first order accurate in time and space. This can in principle be improved to higher order accuracy, although the version here was found sufficient for the purpose of comparison with the hybrid method. The scheme was found to be stable for $\Delta t \lesssim 10^{-3}$ over a wide range of Peclet number and mesh sizes up to 1024×1024.

6.1. Velocity calculation

Calculation of the fluid velocity (66) exterior to the bubble surface is the most expensive component of the traditional method. It requires evaluation of the velocity from (44) at $O(MP)$ grid positions $z(\zeta_{ij})$, where $\zeta_{ij} = r_j e^{iv_i}$ is a discretization of an annular preimage in the unit disk. A naive implementation of the boundary integral method would accomplish this by contour integration, i.e. by evaluation of the Goursat functions $f(\zeta_{ij})$ and $g(\zeta_{ij})$ from (31) and (34), with $I(\zeta_{ij})$ calculated by discretization of the contour integral (32) at a cost of $O(M^2P)$ operations. This can be improved to $O(MP)$ operations using a suitable fast method such as the fast multipole method [54]. As an alternative that can be used with the complex variable and conformal mapping formulation of Stokes flow used here, we describe a new and simple procedure to evaluate the velocity in $O(MP)$ operations using analytic continuation of the boundary values.

Table 1
CPU time to compute a solution at $t = 1$ for timestep $\Delta t = 10^{-3}$.

$M = P$	Traditional	Hybrid
64	15.48	3.13
128	57.58	5.82
256	231.26	17.78
512	1023.50	98.03
1024	4350.96	438.96

The Goursat functions $f(\zeta)$, $g(\zeta)$ are first calculated on the unit disk $\zeta_i = e^{iv_i}$ from Eqs. (31) and (34), respectively (for brevity we write $\zeta_i = \zeta_{i,0}$). Details are given for the evaluation of $f(\zeta_{i,j})$, since the computation of $g(\zeta_{i,j})$ is similar. The discrete Fourier transform of f gives the formula

$$f(\zeta_i) = \sum_{k=-1}^{M-2} \hat{f}_k e^{ikv_i}, \quad i = 1, \ldots, M, \tag{71}$$

where the summation is over $-1 \leqslant k \leqslant M-2$ since $f(\zeta)$ is analytic on the unit disk with the exception of a simple pole at the origin. The analytic continuation of f to the interior of the unit disk, $f(\zeta_{i,j})$ for $j = 1, \ldots, P-1$, is numerically implemented via multiplication of the kth Fourier coefficient by r_j^k, i.e.

$$f(\zeta_{i,j}) = \sum_{k=-1}^{M-2} \hat{f}_k r_j^k e^{ikv_i}, \quad i = 1, \ldots, M. \tag{72}$$

Since $r_j < 1$ this is a well-posed operation. The inverse FFT provides the real space values $f(\zeta_{i,j})$ for $i = 1, \ldots, M$ and fixed j in $O(M \log M)$ operations. Repeating this procedure for each $j = 1, \ldots, P-1$ gives $f(\zeta_{i,j})$ at all gridpoints in $O(MP)$ operations (omitting logarithmic corrections). The Goursat function $g(\zeta)$ and conformal map $z(\zeta)$ are similarly computed for ζ in the interior of the unit disk, and derivatives such as $f_\zeta(\zeta_{i,j})$ and $g_\zeta(\zeta_{i,j})$ are calculated via the DFT. The velocity is then evaluated from (23), where

$$\bar{f}'(\bar{z}) = \frac{\overline{f_\zeta(\zeta_{i,j})}}{\overline{z_\zeta(\zeta_{i,j})}}, \quad \bar{g}\prime(\bar{z}) = \frac{\overline{g_\zeta(\zeta_{i,j})}}{\overline{z_\zeta(\zeta_{i,j})}}. \tag{73}$$

This formulation of a traditional method requires $O(MP)$ operations per time step in 2D flow, which is the same as the current implementation of the hybrid method. Numerical tests summarized in Table 1 reflect the $O(MP)$ dependence of CPU time on the number of gridpoints, and indicate that the implementation of the hybrid method is about 10 times faster than the traditional method.

7. Numerical results

When the surfactant is insoluble ($J = 0$) the method has been validated by comparison with exact steady solutions obtained from complex variable theory. Details of the validation and application of the method on several problems of bubble dynamics with insoluble surfactant, in both steady and unsteady flows, are given in [42].

The implementation of the hybrid method with soluble surfactant ($J > 0$) was checked to have the expected second order accuracy in time and space and was verified by comparing numerical results with analytical solutions. A simple analytical solution describes the unsteady adsorption of surfactant from a spatially uniform bulk state $C = 1$ on to an initially clean bubble surface in the absence of flow when the bubble surface is an infinite sink of surfactant, i.e. $C|_S = 0$ for all t. Agreement between the numerical and analytical solutions is excellent.

As an additional test, we compare with an asymptotic solution of the transition layer and fluid equations, valid for small capillary number $Q \ll 1$ and $E = 0$, which is derived in the Appendix. The solution describes the steady state shape and bulk surfactant concentration for a bubble in an imposed strain, when the surface is an infinite sink of surfactant (i.e. $C|_S = 0$). To leading order in Q, the conformal map parameters and steady surface velocity components are given by

$$a = -1, \quad b = -2Q, \quad u_s = -Q \sin 2v, \quad u_n = 0, \tag{74}$$

and the solution to Eq. (38) for the surfactant concentration C is

$$C(v, N) = \operatorname{erf}\left(\sqrt{Q} N \sin v\right), \tag{75}$$

where the error function $\operatorname{erf}(z) = (2/\sqrt{\pi}) \int_0^z e^{-x^2} dx$. Note that there is a nonuniformity in the concentration as $N \to \infty$ when $v = 0,\ \pi$, i.e. at the bubble ends.

Fig. 1 compares a solution computed with the hybrid numerical method to the asymptotic solution (74) and (75). The hybrid method was run long enough for the dynamics to reach a steady state, and the figure shows the dissolved surfactant

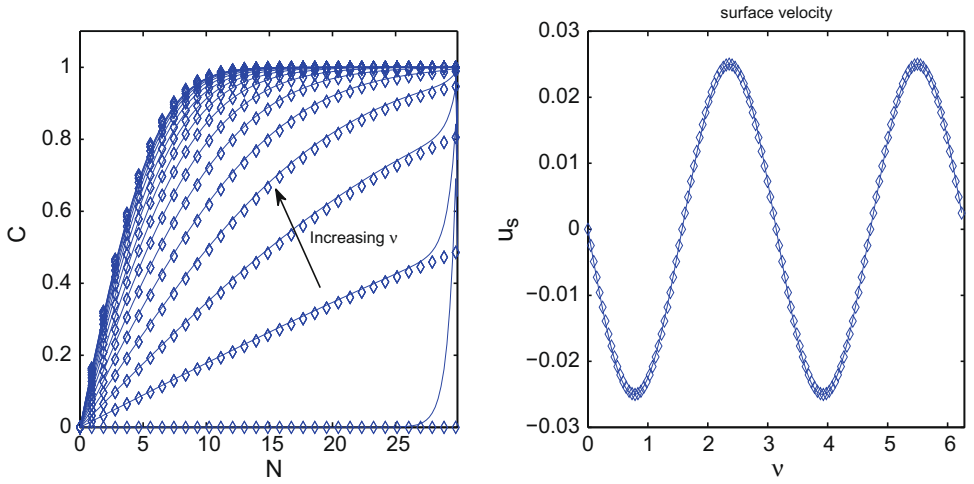

Fig. 1. Comparison of steady solution computed by the hybrid method (solid curves) with the asymptotic solution (74) and (75) (diamonds) for $Q = 0.025$. Left panel: bulk concentration $C(v_i, N)$ for different v_i. Right panel: surface velocity component u_s.

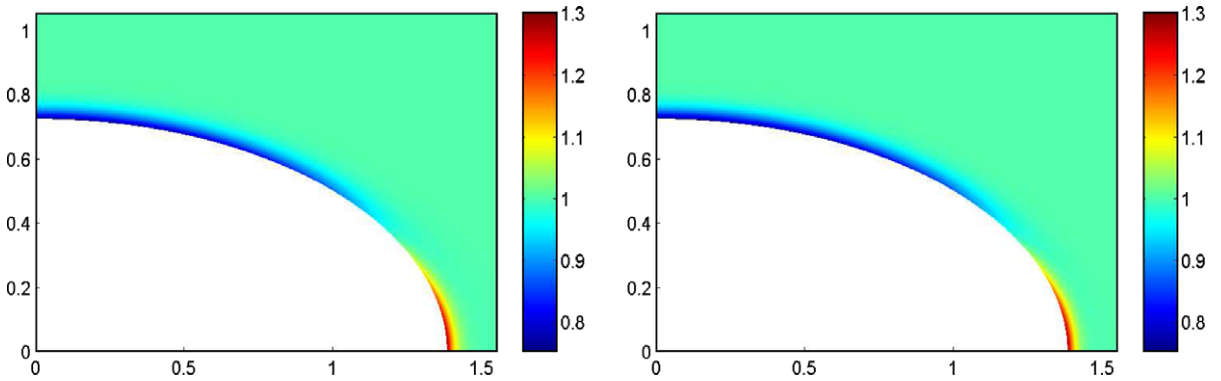

Fig. 2. Bubble shape and bulk surfactant concentration C computed by the hybrid numerical method (left) and traditional method (right). The main physical parameter values are $Pe = 10^3$, $Q = 0.25$, and $t = 1.0$, and computational parameters are $M = P = 256$, $r_m = 0.9$, and $\Delta t = 5.0 \times 10^{-4}$. Good agreement between the two methods is found at this low Pe.

concentration $C(v, N)$ versus the scaled normal coordinate N (left panel, solid curves) at positions $z(v_i)$ $(i = 1, \ldots, 17)$ that are equidistant in v along the bubble surface within one quadrant of the x, y-plane. The solution in the other quadrants follows by symmetry. The lowest solid curve corresponds to $v = 0$, with increasing v indicated in the figure. The diamond markers give the solution (75), and are in excellent agreement with the computed solution. We note that the difference between the two solutions near $N = 30$ is due to the imposition of artificial boundary conditions $C(v, N_m) = 1$ at finite N_m in the computational domain. The numerically computed surface velocity component u_s (Fig. 1, right panel) and bubble shape are indistinguishable to within plotting resolution from the asymptotic values.

The hybrid method is compared in Fig. 2 with the traditional numerical method of Section 6, which uses finite differences on a curvilinear coordinate system exterior to the bubble, without the separate transition layer reduction. The traditional method implemented here retains a degree of adaptivity, since by varying the width r_m of the annular region in the ζ-plane we can cluster gridpoints in a narrow layer adjacent to the bubble surface. We compare the accuracy and efficiency of the hybrid method with this fixed grid, nonadaptive traditional method by fixing $r_m = 0.9$. Fig. 2 shows the shape and bulk surfactant concentration C for an initially circular bubble stretched by a pure strain with capillary number $Q = 0.25$ and $Pe = 10^3$, and indicates good agreement between the two methods at this (physically unrealistic) low value of Pe. Computational parameters are $M = P = 256$ and $\Delta t = 5.0 \times 10^{-4}$, and physical parameter values are $E = 0.1$, $K = 1.5$ and $J_0 = 1$, i.e. $J = 1/Pe^{1/2}$. The initial surface concentration of surfactant is $\Gamma = 0.5$ and the initial bulk concentration of surfactant is $C = 1$. We note that in the hybrid method, M and P can be taken as small as $M = P = 64$ without changing the results to within plotting resolution. For larger Pe, the traditional method with the above parameter values begins to lose accuracy due to inadequate resolution of the transition layer.

Profiles for the bulk surfactant concentration data C of Fig. 2 are shown versus the normal coordinate $n = Pe^{-1/2}N$ in Fig. 3 at fixed locations on the bubble surface as computed by the hybrid method (dashed curves) and the traditional method (solid

curves). This shows that the bulk concentration immediately adjacent to the interface C_S is relatively high at the bubble ends, where surfactant tends to leave the interface, and is relatively low at the mid-section, where surfactant is adsorbed onto the interface from the bulk flow. At this value of $Pe = 10^3$ the profiles found by the two methods are close, and are sufficiently close that there is no discernible difference between them in Fig. 2. The value for the normal derivative $\partial_n C|_S$ as computed by both methods, and hence the bulk-interface surfactant exchange term, is in particularly good agreement.

Fig. 4 shows bubble profiles and bulk surfactant concentration computed by the hybrid method with the same capillary number $Q = 0.25$ as in Fig. 2 but with a larger, more realistic, Peclet number $Pe = 10^4$. The bulk concentration C is shown at times $t = 1.0$ (upper left panel) and $t = 4.0$ (upper right panel), and the bubble shape (lower left panel) and surface

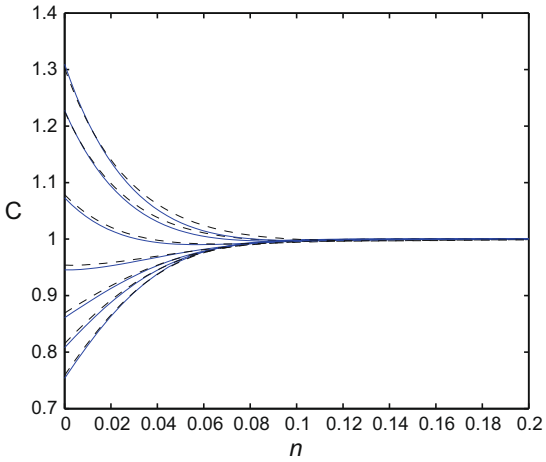

Fig. 3. Bulk surfactant concentration profiles C versus normal coordinate $n = Pe^{-1/2}N$ for the data of Fig. 2. Profiles for the hybrid method are shown by dashed curves and profiles for the traditional method are shown by solid curves. The profiles are plotted at fixed locations on the bubble surface, from $v = 0$ at the bubble end where $C|_S$ is largest to $v = 5\pi/16$ in increments of $\pi/16$ and at the mid-section where $v = \pi/2$.

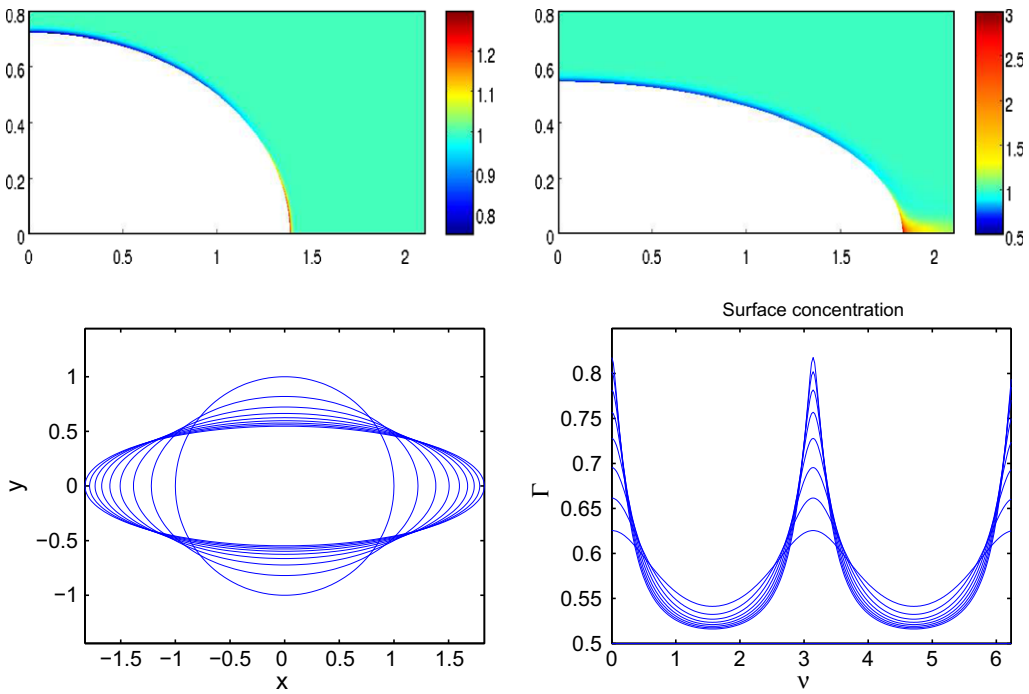

Fig. 4. Evolution of a bubble in a pure strain, computed by the hybrid method with $Pe = 10^4$, $Q = 0.25$, and other parameters as in Fig. 2. Bulk surfactant concentration C at $t = 1.0$ (upper left panel) and $t = 4.0$ (upper right panel), bubble shape (lower left panel) and surface surfactant concentration Γ (lower right panel) plotted from $t = 0.0$ to 4.0 in increments of 0.5.

surfactant concentration Γ (lower right panel) are plotted from $t = 0.0$ to 4.0. Other parameter values are the same as in Fig. 2. The figure clearly illustrates the narrowness of the transition layer at this larger *Pe*, which makes numerical calculation using traditional methods very difficult.

Fig. 5 presents the surface concentration of surfactant $\Gamma(v,t)$ computed by the hybrid method (dotted red curve) and that calculated by the traditional method (solid blue curves) at $t = 1.0$ for $Pe = 0.5 \times 10^2,\ 10^2,\ 10^3,\ 10^4$ and 0.5×10^5. The number of gridpoints is fixed at $M = P = 256$, and other parameters are as in Fig. 2. Since the transition layer Eq. (18) is constructed to be exact in the limit $Pe \to \infty$, we expect solutions computed by the traditional method to approach the hybrid solution for increasing *Pe*. This is indeed the case when the Peclet number *Pe* is less than about 10^3, as seen in Fig. 5. How-

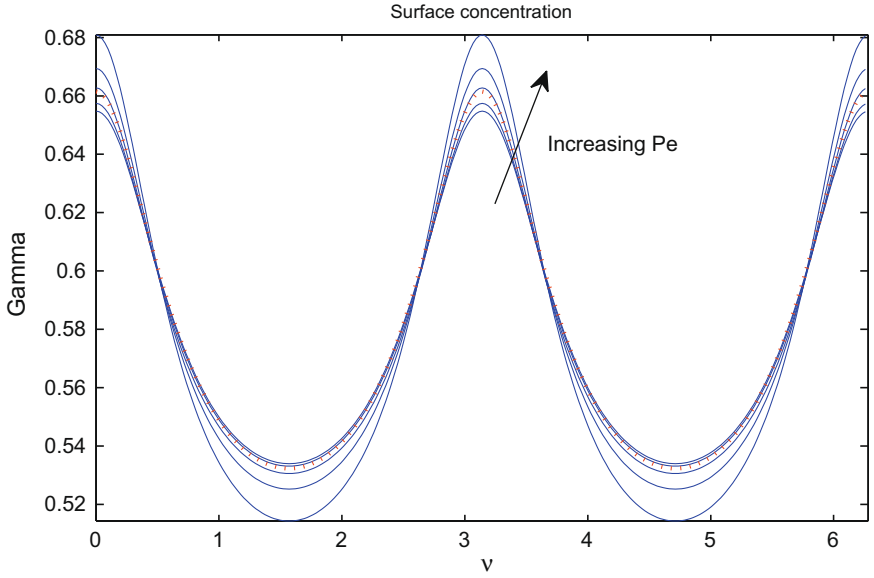

Fig. 5. Surface concentration $\Gamma(v,t)$ computed at $t = 1.0$ by the hybrid method (dotted red curve) and by the traditional method (solid blue curves) for $Pe = 0.5 \times 10^2,\ 10^2,\ 10^3,\ 10^4$ and 0.5×10^5. Parameters are as in Fig. 2. (For interpretation of the references in colour in this figure legend, the reader is referred to the web version of this article.)

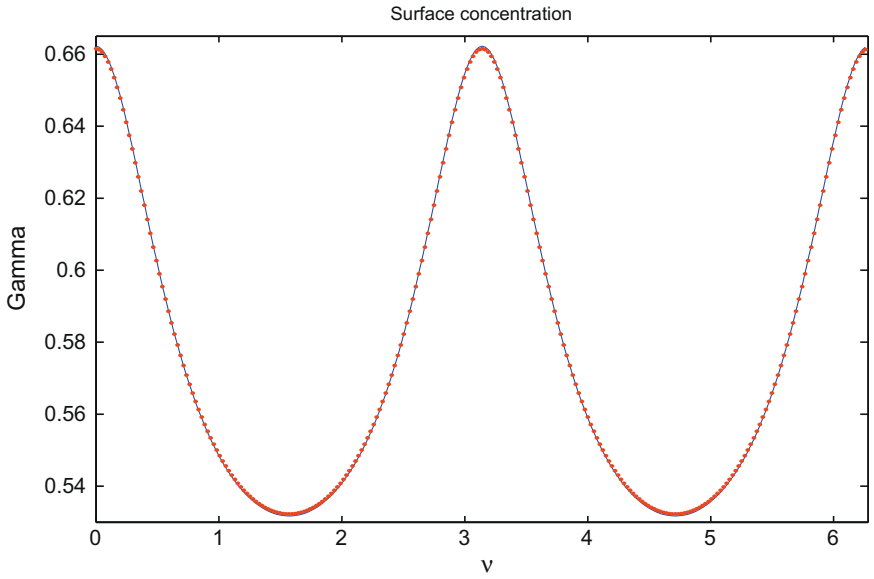

Fig. 6. Surface surfactant concentration $\Gamma(v,t)$ computed by the hybrid method (dotted red curve) and by the traditional method (solid blue curve) at $t = 1.0$ for $Pe = 10^4$. Gridpoints of the traditional method are clustered in a very thin annular region adjacent to the interface by setting $r_m = 0.1$, effectively resolving the transition layer. Other parameters are as in Fig. 2. (For interpretation of the references in colour in this figure legend, the reader is referred to the web version of this article.)

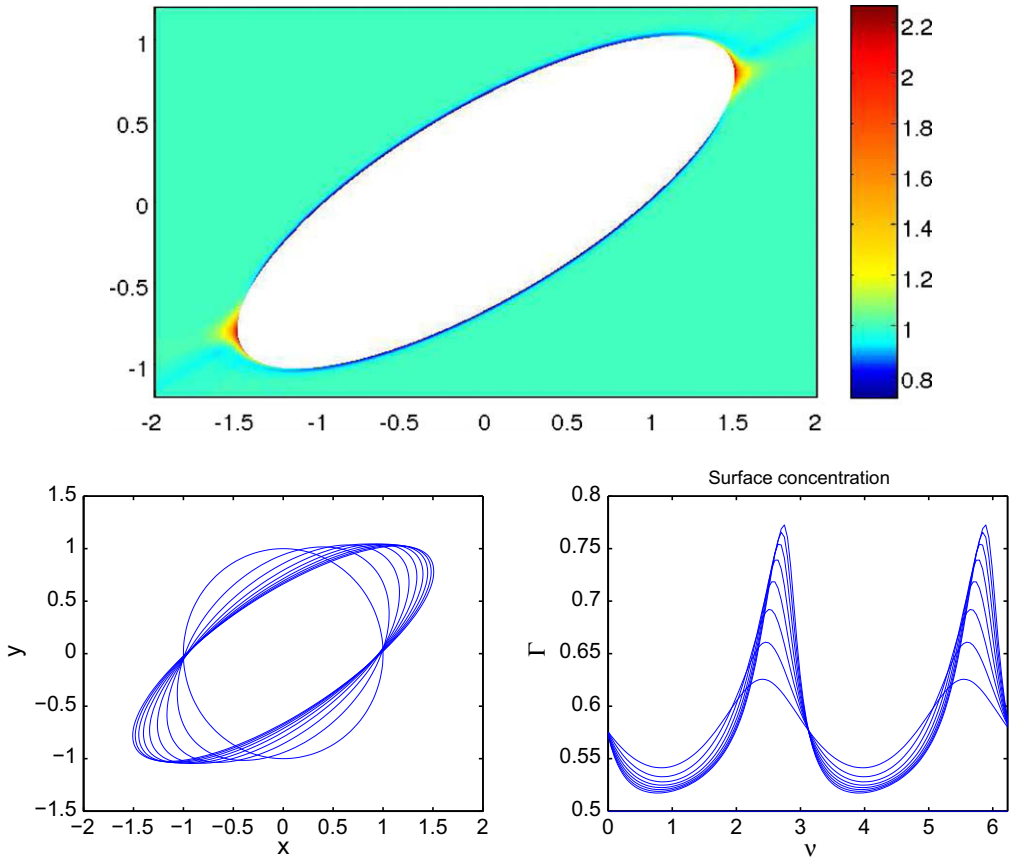

Fig. 7. Evolution of a bubble in a simple shear flow, computed by the hybrid method for $Pe = 10^4$ and $Q(\equiv G) = 0.25$. Bulk surfactant concentration C (upper panel) at $t = 4.0$, bubble shape (lower left panel) and surface concentration Γ (lower right panel) plotted from $t = 0.0$ to 4.0 in increments of 0.5.

ever, when $Pe \gtrsim 10^3$, the traditional method with the present fixed resolution is unable to resolve the large gradients in surfactant concentration near the interface, especially when $\nu \simeq 0, \pi, 2\pi$ (i.e. at the bubble ends), and the profile for Γ with Pe increasing above 10^3 diverges from the expected limiting solution. We improved the accuracy of the solution computed by the traditional method with $Pe = 10^4$ by setting $r_m = 0.1$, so that gridpoints are clustered in a thinner annular layer near the interface. Fig. 6 shows that, at this greatly increased resolution, the traditional and hybrid methods give results that are nearly indistinguishable.

Fig. 7 shows the bulk surfactant concentration C, time-dependent shapes, and surface concentration Γ for a bubble in a simple shear flow, computed by the hybrid method. Main parameter values are $Pe = 10^4$ and $G = -2B = 0.25$, with other parameter values as in Fig. 2. The bubble evolves through a series of elliptical shapes with aspect ratio and orientation that change in time. In both strained and sheared bubbles, the concentration of bulk surfactant at the bubble ends is much higher than at points where the drop surface is flat. This is due to surfactant leaving the bulk flow and adsorbing onto the bubble surface in its middle, flat part, and desorbing from the surface to re-enter the bulk flow at the bubble ends. Surfactant is advected between these regions by the imposed shearing or straining flow. This mechanism of surfactant advection occurs in tipstreaming, and numerical studies of sheared or strained drops with small internal viscosity in the presence of insoluble surfactant that are resolved have been given by Eggleton et al. [3] and Bazhlekov et al. [15].

8. Conclusion

We have presented a hybrid numerical method for the computation of fluid interfaces with soluble surfactant. The method accurately resolves the transition layer adjacent to the interface that occurs in the physically realistic limit of large bulk Peclet number $Pe \to \infty$, in which the surfactant concentration varies rapidly. Faithful resolution of surfactant gradients in the layer is essential for accurate evaluation of surfactant exchange between the interface and bulk fluid, which in turn effects surface tension and interface dynamics.

The behavior in the transition layer is obtained by a singular perturbation analysis of the governing equations near the interface S in the limit $Pe \to \infty$. This uses an intrinsic, i.e. time-dependent, interface-fitted coordinate system with a scaled

normal coordinate $N = n/\epsilon$, where $\epsilon = Pe^{-1/2}$ and ϵ is the spatial scale of the layer width. The pressure and fluid velocity components do not depend on the scaled coordinate N, and the leading order equation for dissolved surfactant C in the transition layer is (18), subject to boundary conditions (19) that $C = C(\Gamma)$ on S and $C \to 1$ as $N \to \infty$.

The tangential fluid velocity at the interface, $\mathbf{u}_s$, and normal derivative of the normal fluid velocity relative to the interface, $\partial_n v_p|_S$, which appear in the transition layer Eq. (18), are evaluated accurately by existing surface based numerical methods, such as the boundary integral or boundary element method. Also, the relation $C = C(\Gamma)$ between surfactant concentration adsorbed on the interface Γ and the neighboring dissolved concentration C is known.

Our implementation of the hybrid numerical algorithm combines a fixed grid numerical solution of the boundary value problem for dissolved surfactant C in the intrinsic coordinate frame with simultaneous boundary integral solution of the problem for $\mathbf{u}$, p, and Γ. This has the advantage that there is no need to re-mesh the grid that is used to solve for C as the interface evolves, even for highly contorted interface shapes. Since the diffusive term $\partial_N^2 C$ is $O(1)$ in the rescaled transition layer Eq. (18), there is no development of large concentration gradients that requires a large number of node points to resolve. The method is effective for arbitrarily large values of Pe.

The algorithm is based on a complex variable formulation of the boundary integral equations for evolution of an inviscid bubble in 2D Stokes flow. The imposed flow that stretches the bubble is an arbitrary linear strain or shear. The method generates the time update of the fluid velocity and surface concentration of surfactant in $O(M)$ operations, where M is the number of discretization points on the bubble surface. Calculation of the bulk surfactant concentration C requires $O(MP)$ operations, where P is the number of gridpoints normal to the interface. There is a Green's function representation of the solution to Eq. (18) for C in the transition layer, which may reduce the operation count, and this is the subject of future work.

The hybrid method has been compared with a more traditional numerical approach that uses finite differences on a moving, body-fitted grid in the fluid region exterior to the bubble, without the separate transition layer reduction. The results are in good agreement for reasonably fine meshes when Pe is less than about 10^3. At larger, more realistic Pe, the traditional method becomes prohibitively expensive due to the separation of scales in the transition layer and the need to accurately resolve its dynamics.

Despite the limitations of a traditional method to unphysically small Pe, the choice of a complex variable, boundary integral conformal mapping technique for the underlying flow solver greatly facilitates computation of surfactant solubility effects by a traditional method. This occurs since (i) analytic continuation and a DFT can be used to accurately and efficiently evaluate the off-surface fluid velocity that appears in the unscaled Eq. (5) for the conservation of dissolved surfactant C. This leads to a traditional method that achieves the same $O(MP)$ operation count as the hybrid method. (ii) The moving, body-fitted grid used to compute C in the z-plane is generated simply as the image under the conformal map of fixed radial gridpoints that are specified in an annulus $0 < 1 - r_m \leqslant |\zeta| \leqslant 1$ of the fixed computational domain $0 \leqslant |\zeta| \leqslant 1$ in the ζ-plane. By decreasing the width of the annulus r_m, gridpoints are readily clustered closer to the interface in the z-plane, and computation can be continued at larger Pe than could be attained otherwise. The conformal mapping technique is however confined to use in 2D flow, and becomes slower and more difficult to implement for a bubble interior that is not inviscid.

The hybrid method for soluble surfactant has been implemented here in low Reynolds number flow, although this is not a limitation. Numerical methods that are designed to solve for moving interfaces in Navier–Stokes flow at intermediate Reynolds numbers, such as the immersed interface or level set method, can be combined with Eq. (18) to accurately capture the dynamics of the transition layer. This extension will be pursued in future work.

Acknowledgments

This work was supported by the NSF under Grant Nos. DMS-0708977 and DMS-0354560. Simulations were conducted on the NJIT computing cluster, supported by the NSF/MRI under Grant No. DMS-0420590. Thanks to Kuan Xu for assistance with the graphics.

Appendix A. *A.1. Steady solution for $Q \ll 1$*

Here we derive the steady state solution (74) and (75) in the limit of small capillary number $Q \ll 1$ with $E = 0$ and $C|_S = 0$. The conformal map $z(\zeta)$ is given by (46) where the map parameters a, b satisfy (47) with $\frac{d}{dt} \equiv 0$. For small Q the bubble is only slightly deformed from a circle, so that b is also small. Evaluating the integral $\widehat{I}_0$ of (41) with $\sigma = 1$ and b small, we find that

$$\widehat{I}_0 = \frac{1}{2|a|} + O(b^2), \tag{76}$$

where the remainder is $O(b^2)$ since for a pure strain $\widehat{I}_0$ and b are real. When (76) is substituted into the steady version of (47), i.e. $Qa = \widehat{I}_0 b$, since a is real and negative, $b = -2Qa^2$ at leading order. Then from the bubble area constraint (48),

$$a = -1 + O(Q^2), \qquad b = -2Q + O(Q^3). \tag{77}$$

The fluid velocity at the interface is computed from (44) and (45) by expanding the map for small b, to give

$$u_1 + iu_2|_S = \frac{ib}{2|a|} e^{-iv} \sin 2v$$

at leading order. The complex velocity $U = u_s + iu_n$ of (36) is therefore

$$U = -Q \sin 2v,$$

which, with (77), gives (74).

The transition layer equation in complex form (38) becomes

$$Q\left(-\sin 2v \frac{\partial C}{\partial v} + 2\cos 2v N \frac{\partial C}{\partial N}\right) = \frac{\partial^2 C}{\partial N^2},$$

to leading order in Q, which in terms of the coordinate $\xi = \cos 2v$ is

$$2Q\left((1-\xi^2)\frac{\partial C}{\partial \xi} + \xi N \frac{\partial C}{\partial N}\right) = \frac{\partial^2 C}{\partial N^2}. \tag{78}$$

The solution sought for C is periodic in ξ, with $C = 0$ on the interface $N = 0$ and $C \to 1$ as $N \to \infty$. Following [55] we look for a similarity solution $C = C(\eta)$ where $\eta = N/\gamma(\xi)$, which leads to the system of equations

$$C_{\eta\eta} = -D\eta C_\eta,$$
$$(\xi^2 - 1)\gamma\gamma_\xi + \xi\gamma^2 = -\frac{D}{2Q},$$

where D is an arbitrary positive constant, and we choose $D = 2$. The solution of this system that satisfies the boundary conditions is

$$C(\eta) = \operatorname{erf}(\eta),$$
$$\gamma^2(\xi) = \frac{(2/Q)(1+\xi) + K}{1-\xi^2},$$

where K is a constant. We choose $K = 0$, so that $\gamma(\xi)$ is finite when $\xi = -1$, since this implies that the solution for C is not identically zero for $N > 0$ at the top and bottom poles of the bubble. In terms of v, this gives $\eta = \sqrt{Q}N \sin v$ and the expression for C of (75).

References

[1] G.I. Taylor, The formation of emulsions in definable fields of flow, Proc. Roy. Soc. Lond. A 146 (1934) 501–523.
[2] R.A. DeBruijn, Tipstreaming of drops in simple shear flows, Chem. Eng. Sci. 48 (1993) 277–284.
[3] C.D. Eggleton, T.-M. Tsai, K.J. Stebe, Tip streaming from a drop in the presence of surfactants, Phys. Rev. Lett. 87 (2001) 048302.
[4] M.R. Booty, M. Siegel, Steady deformation and tip-streaming of a slender bubble with surfactant in extensional flow, J. Fluid Mech. 544 (2005) 243–275.
[5] S.L. Anna, H.C. Mayer, Microscale tipstreaming in a microfluidic flow focusing device, Phys. Fluids 18 (2006) 121512.
[6] Y.T. Hu, D.J. Pine, L.G. Leal, Drop deformation, breakup, and coalescence with compatibilizer, Phys. Fluids 12 (2000) 484–489.
[7] A.B. Branger, D.M. Eckmann, Accelerated arteriolar gas embolism reabsorption by an exogenous surfactant, Anesthesiology 96 (2002) 971–979.
[8] D. Halpern, J.B. Grotberg, Fluid-elastic instabilities of liquid-lined flexible tubes, J. Fluid Mech. 244 (1992) 615–632.
[9] C. Pozrikidis, Boundary Integral and Singularity Methods for Linearized Viscous Flow, Cambridge University Press, Cambridge, 1992.
[10] H.A. Stone, L.G. Leal, The effects of surfactants on drop deformation and breakup, J. Fluid Mech. 222 (1990) 161–186.
[11] W.J. Milliken, H.A. Stone, L.G. Leal, The effect of surfactant on transient motion of Newtonian drops, Phys. Fluids A 5 (1993) 69–79.
[12] Y.Y. Renardy, M. Renardy, V. Cristini, A new volume-of-fluid formulation for surfactants and simulations of drop deformation under shear at a low viscosity ratio, Eur. J. Mech. B 21 (2002) 49–59.
[13] M.A. Drumright-Clarke, Y. Renardy, The effect of insoluble surfactant at dilute concentration on drop breakup under shear with inertia, Phys. Fluids 16 (2004) 14–21.
[14] A.J. James, J. Lowengrub, A surfactant-conserving volume-of-fluid method for interfacial flows with insoluble surfactant, J. Comput. Phys. 201 (2004) 685–722.
[15] I.B. Bazhlekov, P.D. Anderson, H.E.H. Meijer, Numerical investigation of the effect of insoluble surfactants on drop deformation and breakup in simple shear flow, J. Colloid Interf. Sci. 298 (2006) 369–394.
[16] C. Pozrikidis, Numerical studies of singularity formation at free surfaces and fluid interfaces in two-dimensional Stokes flow, J. Fluid Mech. 331 (1997) 145–167.
[17] C. Pozrikidis, Numerical studies of cusp formation at fluid interfaces in Stokes flow, J. Fluid Mech. 357 (1998) 29–57.
[18] M. Siegel, Cusp formation for time-evolving bubbles in two-dimensional Stokes flow, J. Fluid Mech. 412 (2000) 227–257.
[19] A. Borhan, C.-F. Mao, Effect of surfactants on the motion of drops through circular tubes, Phys. Fluids A 4 (1992) 2628–2640.
[20] S. Kwak, C. Pozrikidis, Effect of surfactants on the instability of a liquid thread or annular layer. Part I. Quiescent fluids, Int. J. Multiphase Flow 27 (2001) 1–37.
[21] X. Li, C. Pozrikidis, The effect of surfactants on drop deformation and on the rheology of dilute emulsions in Stokes flow, J. Fluid Mech. 341 (1997) 165–194.
[22] T.M. Tsai, M.J. Miksis, The effects of surfactant on the dynamics of bubble snap-off, J. Fluid Mech. 337 (1997) 381–410.
[23] S. Yon, C. Pozrikidis, A finite volume/boundary-element method for flow past interfaces in the presence of surfactants, with application to shear flow past a viscous drop, Comput. Fluids 27 (1998) 879–902.
[24] M.G. Blyth, H. Luo, C. Pozrikidis, Stability of axisymmetric core-annular flow in the presence of insoluble surfactant, J. Fluid Mech. 548 (2006) 207–235.
[25] M.-C. Lai, Y.-H. Tang, H. Huang, An immersed boundary method for interfacial flows with insoluble surfactant, J. Comput. Phys. 227 (2008) 7279–7293.
[26] J. Lee, C. Pozrikidis, Effect of surfactants on the deformation of drops and bubbles in Navier–Stokes flow, Comput. Fluids 35 (2006) 43–60.
[27] J.-J. Xu, Z. Li, J. Lowengrub, H. Zhao, A level-set method for interfacial flows with surfactant, J. Comput. Phys. 212 (2006) 590–616.
[28] C.H. Chang, E. Franses, Adsorption dynamics of surfactants at the air/water interface: a critical review of mathematical models, data, and mechanisms, Colloids Surf. A 100 (1995) 1–45.
[29] R. Palaparthi, D.T. Papageorgiou, C. Maldarelli, Theory and experiments on the stagnant cap regime in the motion of spherical surfactant-laden bubbles, J. Fluid Mech. 559 (2006) 1–44.

[30] W.J. Milliken, L.G. Leal, The influence of surfactant on the deformation and breakup of a viscous drop: the effect of surfactant solubility, J. Colloid Interf. Sci. 166 (1994) 275–285.
[31] D.M. Leppinen, M. Renksizbulut, R.J. Haywood, The effects of surfactants on droplet behavior at intermediate Reynolds numbers. I: The numerical model and steady state results, Chem. Eng. Sci. 51 (1996) 479–490.
[32] Y. Liao, J.B. McLaughlin, Bubble motion in aqueous surfactant solutions, J. Colloid Interf. Sci. 224 (2000) 297–310.
[33] Y. Liao, J. Wang, R.J. Nunge, J.B. McLaughlin, Comment on bubble motion in aqueous surfactant solutions, J. Colloid Interf. Sci. 272 (2004) 498–501.
[34] Y. Wang, D.T. Papageorgiou, C. Maldarelli, Increased mobility of a surfactant-retarded bubble at high bulk concentrations, J. Fluid Mech. 390 (1999) 251–270.
[35] H. Zhou, V. Cristini, J. Lowengrub, C.W. Macosko, 3D adaptive finite element simulations of deformable drops with soluble surfactant: pair interactions and coalescence, unpublished manuscript.
[36] J. Zhang, D.M. Eckmann, P.S. Ayyaswamy, A front tracking method for a deformable intravascular bubble in a tube with soluble surfactant transport, J. Comput. Phys. 214 (2006) 366–396.
[37] S.N. Ghadiali, D. Halpern, D.P. Gaver, A dual-reciprocity boundary element method for evaluating bulk convective transport of surfactant in free-surface flows, J. Comput. Phys. 171 (2001) 534–559.
[38] M. Muradoglu, G. Tryggvason, A front-tracking method for computation of interfacial flows with soluble surfactants, J. Comput. Phys. 227 (2008) 2238–2262.
[39] R.G.M. van der Sman, S. van der Graaf, Diffuse interface model of surfactant adsorption onto flat and droplet interfaces, Rheol. Acta 46 (2006) 3–11.
[40] F. Jin, N.R. Gupta, K.J. Stebe, The detachment of a viscous drop in a viscous solution in the presence of a soluble surfactant, Phys. Fluids 18 (2006) 022103.
[41] X. Liu, Y. Li, J. Glimm, X.L. Li, A front tracking algorithm for limited mass diffusion, J. Comput. Phys. 222 (2007) 644–653.
[42] M. Siegel, Influence of surfactant on rounded and pointed bubbles in two-dimensional Stokes flow, SIAM J Appl. Math. 59 (1999) 1998–2027.
[43] M. Hameed, M. Siegel, Y.-N. Young, J. Li, M.R. Booty, D.T. Papageorgiou, Influence of insoluble surfactant on the deformation and breakup of a bubble or thread in a viscous fluid, J. Fluid Mech. 594 (2008) 307–340.
[44] H. Wong, D. Rumschitzki, C. Maldarelli, On the surfactant mass balance at a deforming fluid interface, Phys. Fluids 8 (1996) 3202–3204.
[45] D.A. Edwards, H. Brenner, D.T. Wasan, Interfacial Transport Processes and Rheology, Butterworth-Heinemann, Boston, 1991.
[46] M. Matalon, C. Cui, J.K. Bechtold, Hydrodynamic theory of premixed flames: effects of stoichiometry, variable transport coefficients and arbitrary reaction orders, J. Fluid Mech. 487 (2003) 179–210.
[47] J. Yao, S. Stewart, On the dynamics of multi-dimensional detonation, J. Fluid Mech. 309 (1996) 225–275.
[48] S. Tanveer, G.L. Vasconcelos, Time-evolving bubbles in two-dimensional Stokes flow, J. Fluid Mech. 301 (1995) 325–344.
[49] L.K. Antanovskii, Influence of surfactants on a creeping free-boundary flow induced by two counter-rotating horizontal thin cylinders, Eur. J. Mech. B 13 (1994) 73–92.
[50] N.I. Muskhelishvili, Singular Integral Equations, P. Noordhoff, Groningen, 1953.
[51] S.G. Mikhlin, Integral Equations, Pergamon Press, New York, 1957.
[52] W.E. Langlois, Slow Viscous Flow, MacMillan, New York, 1964.
[53] K.W. Morton, D.F. Mayers, Numerical Solution of Partial Differential Equations, Cambridge University Press, Cambridge, 1994.
[54] L. Greengard, V. Rokhlin, A fast algorithm for particle simulations, J. Comput. Phys. 73 (1987) 325–348.
[55] A. Acrivos, J.D. Goddard, Asymptotic expansions for laminar forced-convection heat and mass transfer. Part 1. Low speed flows, J. Fluid Mech. 23 (1965) 273–291.